

Understanding the influence of ENSO on the Great Plains low-level jet in CMIP5 models

James F. Danco¹  · Elinor R. Martin^{1,2}

Received: 13 March 2017 / Accepted: 10 October 2017 / Published online: 28 October 2017
© Springer-Verlag GmbH Germany 2017

Abstract The Great Plains Low-Level Jet (GPLLJ) is an important driver of precipitation and severe weather outbreaks over the US Great Plains and undergoes large inter-annual variability. Therefore, to reliably make predictions and projections of Great Plains precipitation, it is essential for the observed influence of ENSO on the GPLLJ to be understood and simulated accurately by global climate models. This study uses four reanalyses and an ensemble of 42 historical simulations from phase 5 of the Coupled Model Intercomparison Project (CMIP5) to investigate the accuracy of the simulated ENSO–GPLLJ teleconnection. From observations, winter ENSO has a significant negative correlation with the GPLLJ in the following spring and a significant positive correlation with the GPLLJ in the following summer. Here, it is shown that the influence of ENSO is on the frequency, not intensity, of GPLLJ events in the spring, while both the frequency and intensity of GPLLJ events are affected in the summer. However, although the majority of CMIP5 historical simulations exhibit the observed significant negative ENSO–GPLLJ correlations in the spring, nearly all of them fail to simulate the significant positive correlation in the summer. The ability of the models to simulate the ENSO–GPLLJ relationship is attributed to the strength of simulated ENSO events and the associated effects on geopotential heights and atmospheric circulation. These results have implications for the predictability of weather and climate in the Great Plains and suggest that the variability of

the GPLLJ will not be reliably captured in future climate simulations if the magnitude of ENSO events and their impacts are not well represented.

Keywords Great Plains low-level jet · CMIP5 · ENSO

1 Introduction

During the months of March through September, the Great Plains of the United States frequently experiences a nocturnal southerly flow of air from just above the surface to approximately 850 hPa, known as the Great Plains low-level jet (GPLLJ) (Higgins et al. 1997). The GPLLJ is strongest from Texas to Kansas, where a mean southerly flow at 850-hPa is evident from March through September, to the west of 98°W (Fig. 1). The GPLLJ has a large impact on the Great Plains, so developing accurate predictions and projections of the timing, location, and intensity of the GPLLJ is vital for the economy, agriculture, and overall livelihood of the people living there. Understanding the mechanisms that are responsible for controlling the variations in the GPLLJ, as well as the ability of global climate models (GCMs) to simulate them, is crucial for improving predictions and projections.

The GPLLJ significantly increases nocturnal convective precipitation over the Great Plains by transporting moisture from the Gulf of Mexico (GOM) and providing low-level convergence at its northern edges (Stensrud 1996; Higgins et al. 1997; Weaver and Nigam 2008; Weaver et al. 2009). The strength and northward extent of the springtime GPLLJ significantly increased from 1979 to 2012, associated with substantial increases in the frequency and intensity of precipitation in the Northern Plains and decreases in precipitation throughout the Southern Plains (Barandiaran et al.

✉ James F. Danco
jdanco@ou.edu

¹ School of Meteorology, University of Oklahoma, 120 David L. Boren Blvd., Norman, OK 73072, USA

² South Central Climate Science Center, University of Oklahoma, Norman, USA

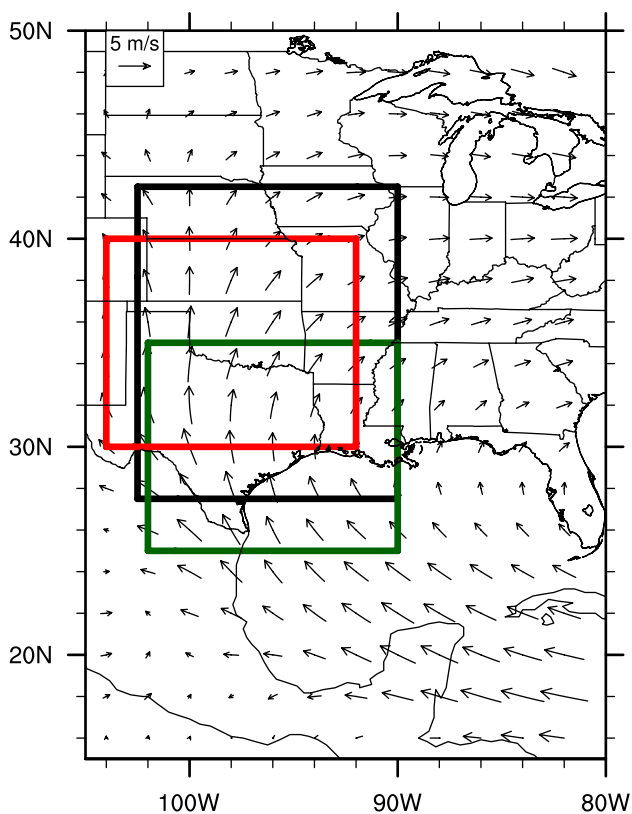


Fig. 1 Mean 850-hPa wind vectors in 20CR from March through September. Boxes illustrate the regions used for the MAM GPLLJ index (green), JAS GPLLJ index (red), and annual GPLLJ index (black)

2013). In addition to effects on precipitation, a more intense GPLLJ results in conditions more conducive to tornado outbreaks across the US, through increased southerly moisture transport from the GOM and greater vertical wind shear (Lee et al. 2013). The GPLLJ is also important for seed dispersion and the migration of birds and insects, which affects agriculture and anyone influenced by the influx of pests and diseases (Stensrud 1996).

Observations have shown that one important influence on the intensity of the GPLLJ are sea surface temperature (SST) anomalies in the equatorial Pacific Ocean, associated with the El Niño–Southern Oscillation (ENSO). Muñoz and Enfield (2011) showed that colder SSTs in the Niño 3.4 region (5°S–5°N, 170°W–120°W) often result in a stronger GPLLJ in the spring, while other studies have found that a warm equatorial Pacific strengthens the GPLLJ in the summer (Schubert et al. 2004; Weaver et al. 2009). These results have significant implications for the predictability of the GPLLJ because they demonstrate that if the state of ENSO can be known in advance, the intensity of the GPLLJ can be predicted.

Krishnamurthy et al. (2015) found that one of the mechanisms that plays a major role in this shift from negative to

positive correlations between ENSO and the GPLLJ from the spring to summer is the Caribbean low-level jet (CLLJ). Studies have shown a positive correlation between the CLLJ and GPLLJ (Cook and Vizy 2010; Martin and Schumacher 2011). Observations indicate wintertime La Niña induces high sea level pressure (SLP) anomalies over the Intra-Americas Sea (IAS) the following spring through changes in the Walker and Hadley circulation. This leads to a strong CLLJ, which drives a stronger GPLLJ. In the summer, however, an El Niño is associated with low SLP anomalies in the tropical Pacific and high SLP anomalies in the tropical Atlantic. This strong SLP gradient results in a stronger CLLJ, which again leads to a stronger GPLLJ. In addition to this tropical link, it has been hypothesized that ENSO can affect the GPLLJ through an extratropical wave train from the tropical west Pacific into North America (Krishnamurthy et al. 2015).

It is known that GCMs are unable to represent some of the features of the GPLLJ in their historical simulations. Sheffield et al. (2013) compared the GPLLJ simulation in eight models from phase 5 of the Coupled Model Intercomparison Project (CMIP5) to the NCEP-NCAR reanalysis. The models place the peak of the GPLLJ at about 925 hPa, while the reanalysis has it at 850 hPa. The simulated GPLLJ also extends farther north compared to the reanalysis, and the models extend the peak of the GPLLJ into late July while the reanalysis weakens it by early July (Sheffield et al. 2013). Cook et al. (2008) also discovered that the prior generation of GCM's simulate a GPLLJ that is too weak in their twentieth-century simulations.

GCM's also struggle with simulating the strength and structure of ENSO, which we hypothesize to influence their ability to represent the correct impact of ENSO on the GPLLJ. Kim and Yu (2012) evaluated 20 CMIP5 models and found that only nine of them can simulate realistically strong ENSO intensities in their preindustrial simulations. The tendency for the strongest El Niños to be stronger than the strongest La Niñas is a problem in CMIP5 models as well (Zhang and Sun 2014). Krishnamurthy et al. (2015) found that the GFDL FLOR coupled climate model simulates too much ENSO variability and inaccurate phase locking, which results in a negative ENSO–GPLLJ correlation in both the spring and summer seasons, in contrast to observations.

Future variability in the intensity and timing of the GPLLJ, and thus in precipitation and severe weather over the Great Plains, cannot be reliably projected if the features and mechanisms of the GPLLJ are not understood and simulated correctly by GCMs. Therefore, an understanding of the relationship between the GPLLJ and ENSO is crucial, in order to improve near- and long-term predictions and projections of Great Plains weather and climate. While some studies have examined the ability of GCMs to simulate the climatology of the GPLLJ, little focus has been given on

their ability to represent its variability at a process-level. This study investigates the features of the GPLLJ and its relationship with ENSO in CMIP5 models.

Section 2 includes a description of the observed data, reanalyzes, and model output, and a discussion of the methodology. Section 3 examines the climatology of the GPLLJ in the CMIP5 models. Section 4 discusses the relationship between ENSO and the GPLLJ in observations and the ability of the CMIP5 models to simulate it. Section 5 demonstrates factors affecting the models' ability to represent the accurate ENSO–GPLLJ relationship and Sect. 6 summarizes and discusses the findings of the study.

2 Data and methodology

The GPLLJ climatology analysis uses monthly meridional wind data from historical simulations (1900–2005) (Taylor et al. 2012) from 42 coupled atmosphere–ocean general circulation models, with 131 individual ensemble members coordinated under CMIP5 (Table 1). Further analysis of zonal wind, SLP, and geopotential heights, only uses 31 of the original 42 models due to data availability issues. The model resolution varies (Table 1), so to facilitate comparison, output was interpolated to a common 2° by 2° latitude–longitude grid using bilinear interpolation. Model averages were obtained by averaging over all ensemble members first, to avoid a bias toward the models with many ensemble members. This CMIP5 model mean will be referred to as the model mean throughout this study.

The model output is compared to monthly data from four reanalyzes: the Twentieth Century Reanalysis version 2c (20CR: $2^\circ \times 2^\circ$, 1900–2014, Compo et al. 2011), ECMWF twentieth century reanalysis (ERA20C: $1^\circ \times 1^\circ$, 1900–2010, Poli et al. 2016), ECMWF interim reanalysis (ERA-Interim: $0.75^\circ \times 0.75^\circ$, 1979–2015, Simmons et al. 2014), and NCEP Climate Forecast System Reanalysis (CFSR: $0.5^\circ \times 0.5^\circ$, 1979–2009, Saha et al. 2010). Six-hourly meridional wind data from ERA-Interim and three CMIP5 models (CNRM-CM5, FGOALS-g2, and MIROC-ESM) is used in Sect. 4c. Only three models were used because of limited access to CMIP5 6-h wind data.

Monthly SST observations (1900–2015) are from the Hadley Centre Global Sea Ice and Sea Surface Temperature dataset (HadISST1: $1^\circ \times 1^\circ$, Rayner et al. 2003). ENSO is measured using the Oceanic Niño Index (ONI), defined as the 3-month running mean of SST anomalies in the Niño 3.4 region using a base period of 1971–2000 (Eichler and Higgins 2006). An ENSO event is defined as having SST anomalies at least one standard deviation from the mean, which is used to facilitate comparison between models that may have differing magnitudes of ENSO variability.

The definition of the annual GPLLJ index is the same as that used by Harding and Snyder (2015); the area-averaged 850-hPa meridional wind speed over 27.5° – 42.5° N, 102.5° – 90° W (Fig. 1; black box). Cook et al. (2008) demonstrate that the GPLLJ is not stationary in space, shifting north from the spring to the summer, so two different regions are used for the spring and summer GPLLJ index. The regions were chosen based on where the GPLLJ is strongest in the 20CR. The March–April–May (MAM) GPLLJ index is defined over 25° – 35° N, 102° – 90° W (Fig. 1; green box), and the July–August–September (JAS) GPLLJ index is defined over 30° – 40° N, 104° – 92° W (Fig. 1; red box).

3 Model evaluation of GPLLJ climatology

Before examining the ENSO teleconnection of the GPLLJ, it is necessary to understand the ability of the CMIP5 models to simulate the climatology of the GPLLJ because accurately representing GPLLJ climatology may be crucial to representing its variability. If the models are unable to simulate features of the GPLLJ itself (e.g. strength, annual cycle, vertical structure), it is unlikely they will be capable of simulating its observed teleconnection with ENSO.

3.1 Annual cycle

The annual cycle of the GPLLJ index from the reanalyzes and CMIP5 model mean is shown in Fig. 2. All four reanalyzes agree on the timing of the GPLLJ, with the peak in June, consistent with previous studies (Cook et al. 2008; Sheffield et al. 2013). The model mean extends its peak from June through August while the reanalyzes sharply weaken it after June. This agrees with the results from Sheffield et al. (2013) which only used eight CMIP5 models. The GPLLJ in the models is too weak throughout the year, except during JAS, consistent with the findings from Cook et al. (2008). The model mean is greater than one standard deviation below the reanalysis mean during all months of the year except from June through September.

To determine the robustness of this model mean result, a statistical analysis is performed to determine the ability of each CMIP5 model to simulate the strength of the GPLLJ using the difference between the modeled and observed 850-hPa meridional wind at each grid point over the MAM and JAS GPLLJ regions. The 20CR is used for the observed GPLLJ because it covers similar years to the CMIP5 models, and the strength of the GPLLJ in the 20CR agrees very closely with the ERA-Interim and CFSR when examining the years they have in common (not shown). These differences (errors) are bootstrapped 1000 times for each model, and a 95% confidence interval is evaluated for these differences to determine if each model error is significant.

Table 1 List of CMIP5 models included in the analysis and their attributes

Model number	Model name	Modeling center	Number of ensemble members	Horizontal resolution (° latitude by ° longitude)	Reference	Subset
1	BCC-CSM1.1	Beijing Climate Center, China Meteorological Administration	3	2.8125×2.8125	Xin et al. (2012)	
2	BCC-CSM1.1-M	Beijing Climate Center, China Meteorological Administration	3	1.125×1.125	Xin et al. (2012)	
3	CanESM2	Canadian Centre for Climate Modeling and Analysis	5	2.8125×2.8125	Arora et al. (2011)	
4	CCSM4	National Center for Atmospheric Research	6	0.9375×1.25	Gent et al. (2011)	
5	CESM1-BGC	Community Earth System Model Contributors	1	0.9375×1.25	Long et al. (2013)	
6	CESM1-CAM5	Community Earth System Model Contributors	3	0.9375×1.25	Meehl et al. (2013)	
7	CESM1-FASTCHEM	Community Earth System Model Contributors	3	0.9375×1.25	Perez et al. (2014)	
8	CESM1-WACCM	Community Earth System Model Contributors	1	1.875×2.5	Marsh et al. (2013)	
9	CMCC-CESM	Centro Euro-Mediterraneo per I Cambiamenti Climatici	1	3.75×3.75	Perez et al. (2014)	X
10	CMCC-CM	Centro Euro-Mediterraneo per I Cambiamenti Climatici	1	0.75×0.75	Perez et al. (2014)	X
11	CMCC-CMS ++	Centro Euro-Mediterraneo per I Cambiamenti Climatici	1	1.875×1.875	Perez et al. (2014)	X
12	CNRM-CM5	Centre National de Recherches Météorologiques/Centre Européen de Recherche et Formation Avancée en Calcul Scientifique	10	1.40625×1.40625	Voldoire et al. (2013)	X
13	CNRM-CM5-2 ++	Centre National de Recherches Météorologiques/Centre Européen de Recherche et Formation Avancée en Calcul Scientifique	1	1.40625×1.40625	Voldoire et al. (2013)	X
14	CSIRO-Mk3L-1-2	Commonwealth Scientific and Industrial Research Organization in collaboration with Queensland Climate Change Centre of Excellence	3	3.2×5.625	Phipps et al. (2011)	
15	FGOALS-g2	LASG, Institute of Atmospheric Physics, Chinese Academy of Sciences and CESS, Tsinghua University	5	3.0×2.8125	Li et al. (2013)	X
16	FGOALS-s2 +	LASG, Institute of Atmospheric Physics, Chinese Academy of Sciences	2	1.7×2.8125	Bao et al. (2012)	X

Table 1 (continued)

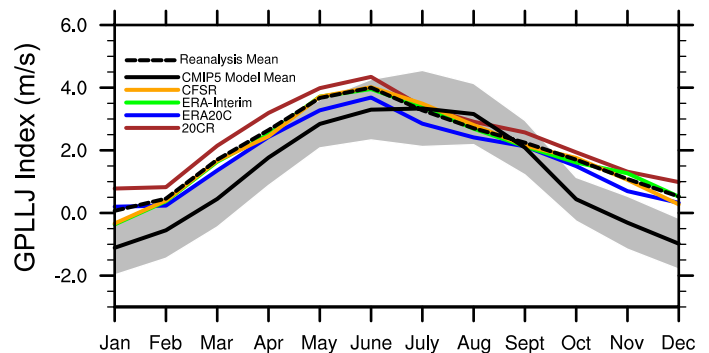
Model number	Model name	Modeling center	Number of ensemble members	Horizontal resolution (° latitude by ° longitude)	Reference	Subset
17	GFDL-CM2.1 + *	NOAA Geophysical Fluid Dynamics Laboratory	10	2.0×2.5	Delworth et al. (2006)	X
18	GFDL-CM3	NOAA Geophysical Fluid Dynamics Laboratory	5	2.0×2.5	Donner et al. (2011)	X
19	GFDL-ESM2G	NOAA Geophysical Fluid Dynamics Laboratory	1	2.0×2.5	Donner et al. (2011)	X
20	GFDL-ESM2M + *	NOAA Geophysical Fluid Dynamics Laboratory	1	2.0×2.5	Donner et al. (2011)	X
21	GISS-E2-H *	NASA Goddard Institute for Space Studies	5	2.0×2.5	Kim et al. (2012)	X
22	GISS-E2-H-CC *	NASA Goddard Institute for Space Studies	1	2.0×2.5	Kim et al. (2012)	X
23	GISS-E2-R +	NASA Goddard Institute for Space Studies	3	2.0×2.5	Kim et al. (2012)	X
24	GISS-E2-R-CC +	NASA Goddard Institute for Space Studies	1	2.0×2.5	Kim et al. (2012)	X
25	HadCM3	Met Office Hadley Centre	10	2.5×3.75	Collins et al. (2001)	X
26	HADGEM2-AO +	National Institute of Meteorological Research/ Korea Meteorological Administration	1	1.25×1.875	Baek et al. (2013)	X
27	HADGEM2-CC	Met Office Hadley Centre	1	1.25×1.875	Jones et al. (2011)	X
28	HADGEM2-ES	Met Office Hadley Centre	5	1.25×1.875	Jones et al. (2011)	X
29	INM-CM4.0 * *	Institute for Numerical Mathematics	1	1.5×2.0	Volodin et al. (2010)	X
30	IPSL-CM5A-LR	Institut Pierre-Simon Laplace	6	1.875×3.75	Dufresne et al. (2013)	X
31	IPSL-CM5A-MR	Institut Pierre-Simon Laplace	3	1.25×2.5	Dufresne et al. (2013)	X
32	IPSL-CM5B-LR *	Institut Pierre-Simon Laplace	1	1.875×3.75	Dufresne et al. (2013)	X
33	MIROC5	Atmosphere and Ocean Research Institute (The University of Tokyo), National Institute for Environmental Studies, and Japan Agency for Marine-Earth Science and Technology	5	1.40625×1.40625	Watanabe et al. (2010)	X
34	MIROC-ESM*	Japan Agency for Marine-Earth Science and Technology, Atmosphere and Ocean Research Institute (The University of Tokyo), and National Institute for Environmental Studies	3	2.8125×2.8125	Watanabe et al. (2010)	X
35	MIROC-ESM-CHEM*	Japan Agency for Marine-Earth Science and Technology, Atmosphere and Ocean Research Institute (The University of Tokyo), and National Institute for Environmental Studies	1	2.8125×2.8125	Watanabe et al. (2010)	X

Table 1 (continued)

Model number	Model name	Modeling center	Number of ensemble members	Horizontal resolution ($^{\circ}$ latitude by $^{\circ}$ longitude)	Reference	Subset
36	MPI-ESM-LR	Max-Planck-Institut für Meteorologie (Max Planck Institute for Meteorology)	3	1.875×1.875	Zanchettin et al. (2013)	X
37	MPI-ESM-MR	Max-Planck-Institut für Meteorologie (Max Planck Institute for Meteorology)	3	1.875×1.875	Zanchettin et al. (2013)	X
38	MPI-ESM-P *	Max-Planck-Institut für Meteorologie (Max Planck Institute for Meteorology)	2	1.875×1.875	Zanchettin et al. (2013)	X
39	MRI-CGCM3	Meteorological Research Institute	5	1.125×1.125	Yukimoto et al. (2012)	X
40	MRI-ESM1	Meteorological Research Institute	1	1.125×1.125	Adachi et al. (2013)	X
41	NorESM1-M	Norwegian Climate Centre	3	1.875×2.5	Bentsen et al. (2013)	
42	NorESM1-ME	Norwegian Climate Centre	1	1.875×2.5	Bentsen et al. (2013)	

The last column is marked with an “X” if the model is included in the subset of 31 models used for the additional analysis. The five best (worst) spring models, defined as the five models out of the subset with the strongest (weakest) negative DJF ENSO–MAM GPLLJ correlation, are indicated by + (*). The five best (worst) summer models, defined as the five models out of the subset with the strongest positive (negative) DJF ENSO–JAS GPLLJ correlation, are indicated by + (*).

Fig. 2 Annual cycle of the GPLLJ index for 20CR, ERA20C, ERA-Interim, CFSR, reanalysis mean, and CMIP5 model mean. The gray shading indicates \pm one standard deviation above and below the model mean



As shown in Fig. 3, all models simulate a MAM GPLLJ that is too weak, and 25 out of the 42 models (~60%) have a MAM GPLLJ that is significantly weaker than the 20CR. The median, quartiles, and outliers for every model are less than zero, with the median errors ranging from approximately -0.5 to -2.5 m s^{-1} . However, in JAS (Fig. 4), the model mean GPLLJ is not significantly different from the 20CR and the GPLLJ magnitude differences are much less than in MAM. Only six of the 42 models (~14%) have a GPLLJ that is significantly weaker than the reanalysis, while three models (~7%) have a significantly stronger GPLLJ. The median bootstrapped error is greater than zero for 14 (one-third) of the models, and the median errors range from approximately -2 to 2 m s^{-1} , in contrast to MAM when all

the models have a GPLLJ that is too weak. These results indicate much better model performance in simulating the strength of the GPLLJ in JAS compared to MAM. However, this is because the models extend the peak of the GPLLJ too late in the summer. Consistent with our understanding of the GPLLJ, the models with the weakest GPLLJ exhibit a weaker SLP gradient over the Great Plains than those with the strongest GPLLJ (not shown).

3.2 Diurnal cycle

Figure 5a shows the diurnal cycle of the MAM GPLLJ index in three CMIP5 models and ERA-Interim. As expected, the GPLLJ is strongest in the ERA-Interim at

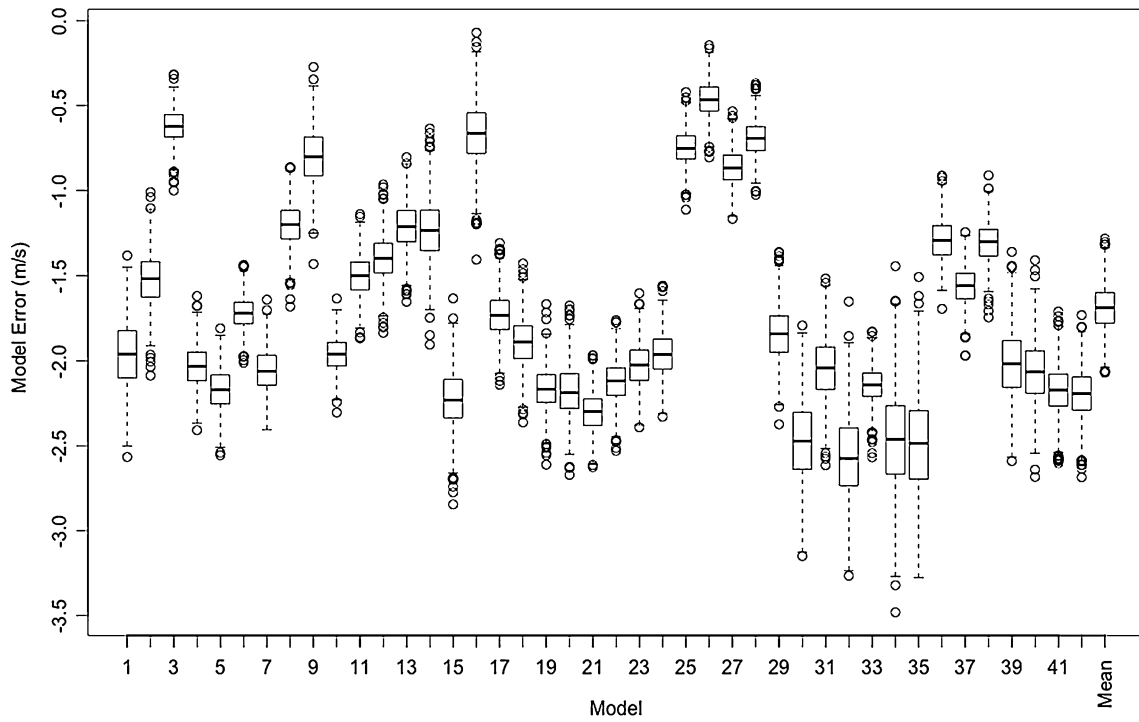


Fig. 3 Boxplots of the bootstrapped differences ($R = 1000$) between the MAM GPLLJ in 42 CMIP5 models and 20CR. The index for each model shown on the horizontal axis is given in Table 1

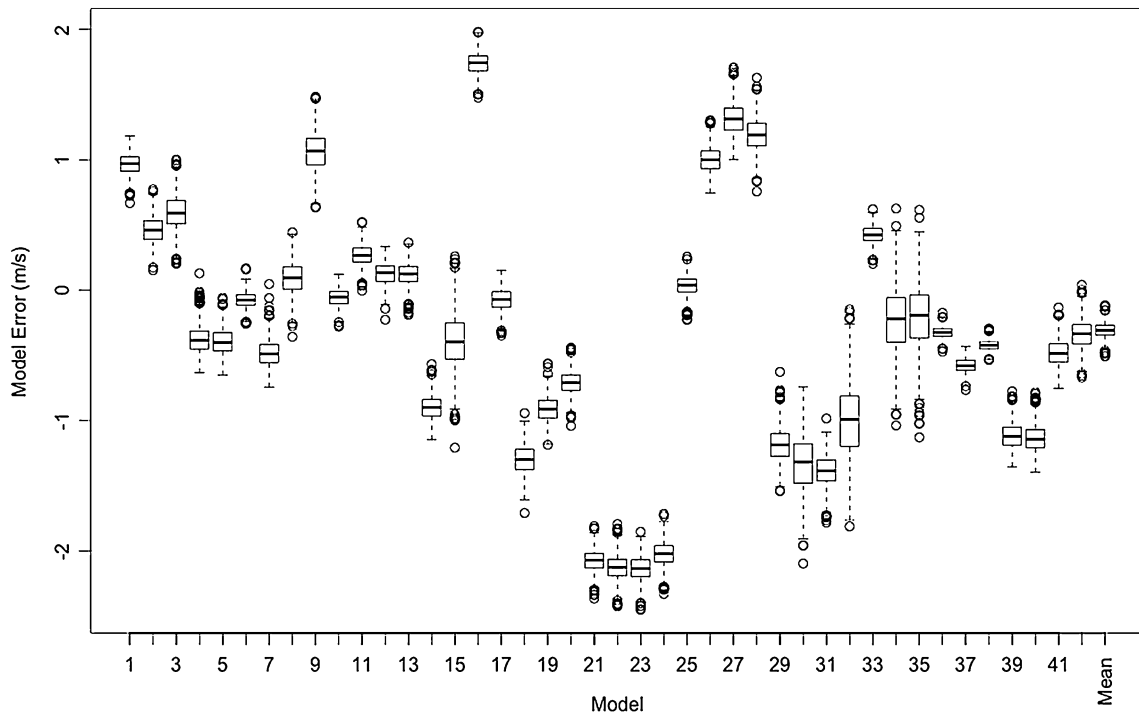


Fig. 4 Same as Fig. 3, but for JAS

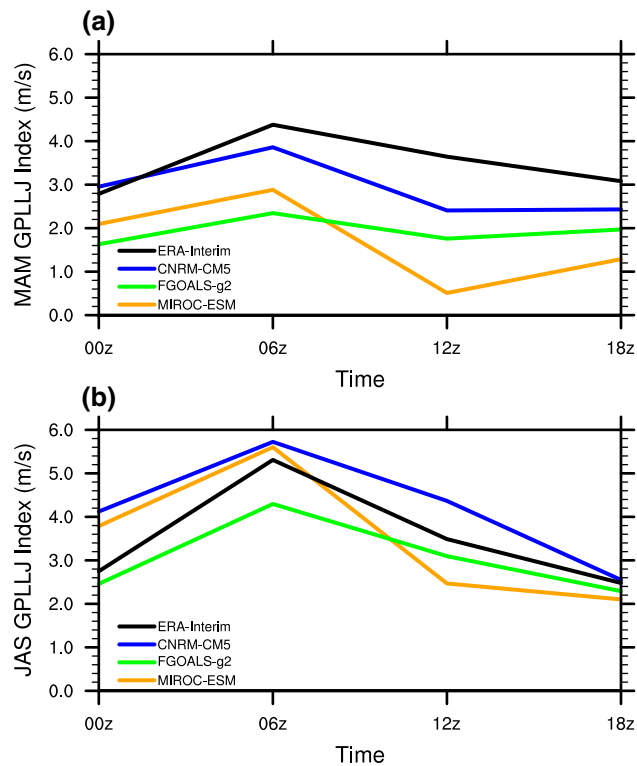


Fig. 5 Diurnal cycle of the MAM (a) and JAS (b) GPLLJ index in ERA-Interim, CNRM-CM5, FGOALS-g2, and MIROC-ESM

06Z (Higgins et al. 1997; Jiang et al. 2007, Pu and Dickinson 2014). Overall, the diurnal cycle in the models compares well to the reanalysis, with the observed peak in the MAM GPLLJ at 06Z. However, the minimum strength of the MAM GPLLJ in ERA-Interim occurs at 00Z, while in the CNRM-CM5 and MIROC-ESM models the GPLLJ is weakest at 12Z. Results for JAS (Fig. 5b) are largely consistent with MAM.

3.3 Vertical structure

To evaluate the ability of the CMIP5 models to represent the vertical structure of the GPLLJ, a vertical profile of the MAM meridional winds over the Great Plains, averaged over 25°–35°N, is shown for 20CR (Fig. 6a), CFSR (Fig. 6b), and the CMIP5 model mean (Fig. 6c). Both reanalyses place the jet at similar longitudes (peaking at 97°–98°W) and levels (peaking at ~900 hPa), but the GPLLJ in the 20CR is 0.5–1 m s⁻¹ stronger at all levels. The models simulate a MAM GPLLJ that is too weak by 1–2 m s⁻¹ throughout the vertical extent of the GPLLJ. The core of the GPLLJ is also located at a lower level in the troposphere (~925 hPa) than it is in the reanalyses (~900 hPa). These results are consistent with the findings of Sheffield et al. (2013) that used fewer models. The models place the GPLLJ farther east than the reanalyses by 1°–2° longitude, peaking it at 96°W. These

biases could be due to horizontal and vertical resolutions in the models that are too coarse, making them unable to represent complex orographic features or planetary boundary layer mechanisms such as those proposed by Blackadar (1957) and Holton (1967).

The JAS vertical profile, averaged over 30°–40°N, is shown in Fig. 6d–f. The 20CR (Fig. 6d) has a similar GPLLJ position and intensity to the CFSR (Fig. 6e) at most levels, but the peak GPLLJ in the CFSR is approximately 1 m s⁻¹ stronger. The model mean GPLLJ (Fig. 6f) is weaker than both reanalyses by approximately 0.5–1 m s⁻¹, which is less than in MAM. As in the spring, the models place the peak wind too far east (by ~2°–3° longitude) and at a lower level in the troposphere (~925 hPa) than in the reanalyses (~850–875 hPa).

4 ENSO–GPLLJ relationship

4.1 ENSO–GPLLJ correlation

To examine the ENSO–GPLLJ mechanism in the models, the lagged cross-correlation between anomalies of the MAM GPLLJ index and previous December–January–February (DJF) ENSO in the 20CR, ERA20C, ERA-Interim, and CFSR are shown in Table 2, along with the model mean correlation. All four reanalyses have a negative correlation (significant at the 95% confidence level), agreeing with Muñoz and Enfield (2011) and Krishnamurthy et al. (2015). This suggests that a La Niña-like state in the tropical Pacific Ocean during winter is associated with a stronger GPLLJ in the following spring, while the opposite is true for El Niño. The model mean correlation is also significantly negative, but it is weaker than it is in the reanalyses.

To examine the spread in the DJF ENSO–MAM GPLLJ relationship among all the CMIP5 models, the standardized least-squares regression lines representing this relationship for each of the 131 ensemble members are shown in Fig. 7a. Overall, 82 out of the 131 ensemble members (~63%) simulate a significant negative correlation, indicating that a majority can capture the observed relationship between ENSO and the GPLLJ in the spring. One ensemble member (from MIROC-ESM) simulates a significant positive correlation, while the rest are insignificant.

Table 2 also shows the correlation between anomalies of the JAS GPLLJ index and previous DJF ENSO in the four reanalyses and model mean. All reanalyses demonstrate a shift to a positive correlation, meaning that a winter El Niño is associated with a stronger GPLLJ in the following summer (Schubert et al. 2004; Weaver et al. 2009; Krishnamurthy et al. 2015). The correlation is significant in the

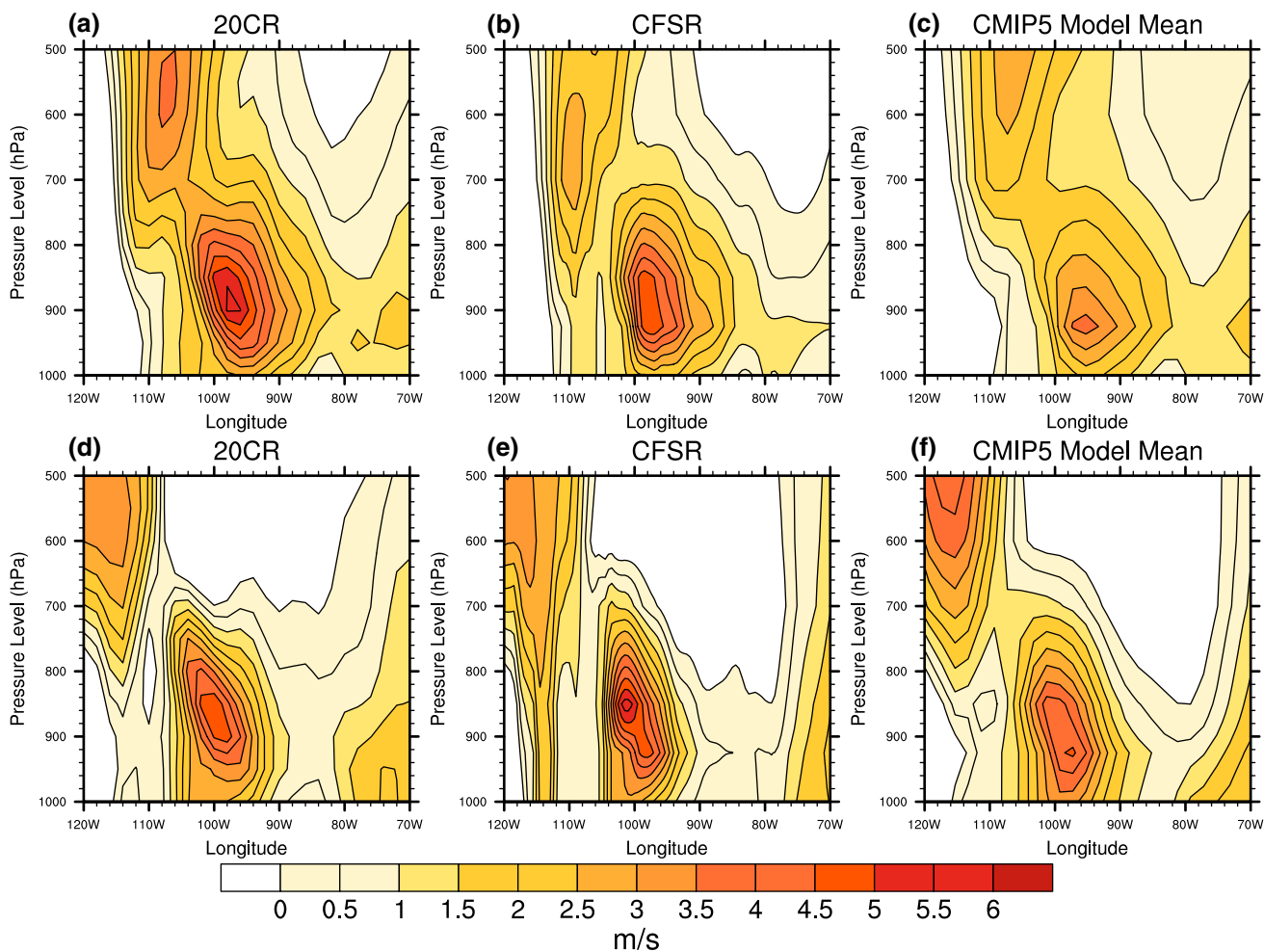


Fig. 6 Lower-tropospheric mean vertical profile of MAM meridional wind averaged over 25°–35°N for 20CR (a), CFSR (b), and CMIP5 model mean (c). The vertical profile of JAS meridional wind averaged over 30°–40°N for 20CR (d), CFSR (e), and CMIP5 model mean (f)

Table 2 Linear cross-correlation between the DJF ENSO and following seasonal GPLLJ anomaly in MAM and JAS

	20CR	ERA20C	ERA-Interim	CFSR	CMIP5 Model mean
MAM	-0.36	-0.40	-0.36	-0.37	-0.24
JAS	0.28	0.29	0.25	0.18	-0.08

All correlations significant at the 95% confidence level using a two-tailed t-test are bolded

20CR and ERA20C but not in the ERA-Interim and CFSR, which may be attributed to the latter two reanalyses covering fewer years. In contrast to the spring, the CMIP5 models are mostly unable to accurately simulate the ENSO–GPLLJ relationship in the summer, as the model mean correlation is very weakly negative.

Standardized regression lines representing the DJF ENSO – JAS GPLLJ relationship for each ensemble

member are displayed in Fig. 7b. A shift toward a less negative correlation from the spring to the summer is apparent in the models, but 28 ensemble members (~21%) still simulate a significant negative correlation, and only two ensemble members (from BCC-CSM1.1-M and FGOALS-g2) simulate the significant positive correlation that is seen in the reanalyses. Furthermore, not a single model mean has a significant positive correlation. These results demonstrate that the CMIP5 models do a very poor job representing the effects of ENSO on the GPLLJ in the summer. It is crucial that causes for this error are determined in order to improve our ability to understand and predict the summer GPLLJ in the future.

4.2 Spatial correlation

To examine the spatial extent and variability of the relationship between ENSO and the GPLLJ, the spatial correlation between DJF ENSO and the following MAM 850-hPa

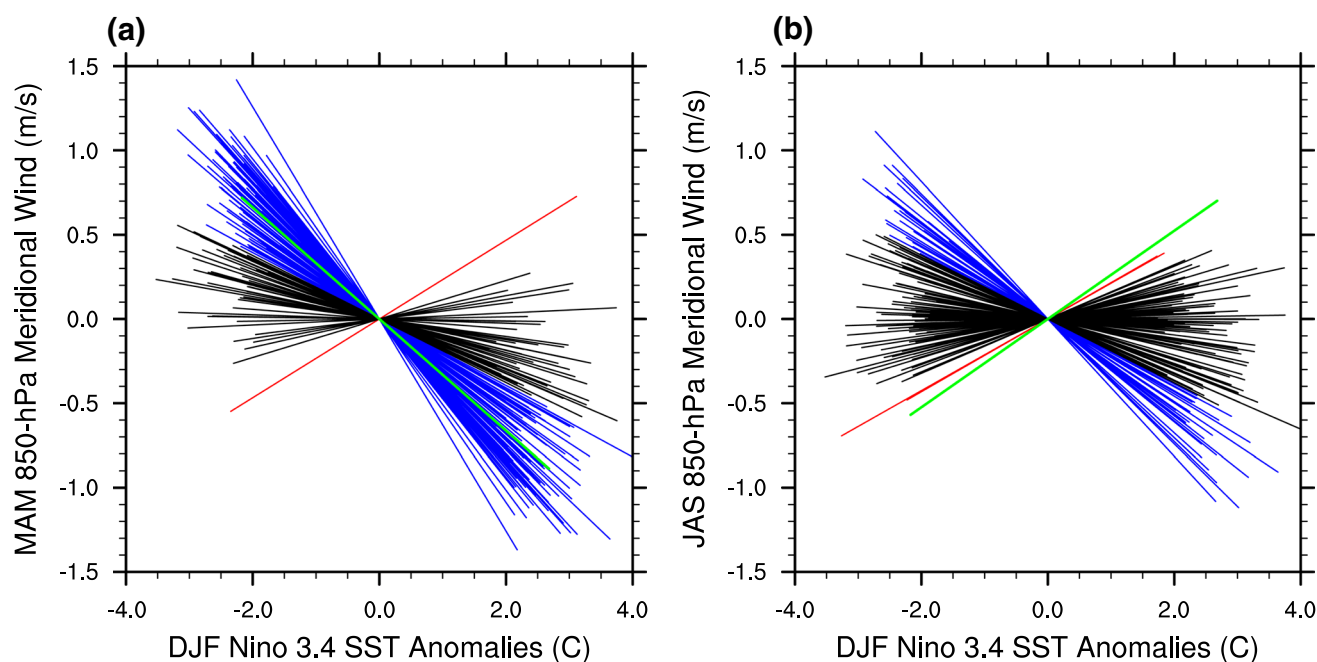


Fig. 7 Standardized least-squares regression lines for each ensemble member representing the relationship between DJF ENSO and GPLLJ anomaly in the following MAM (a) and JAS (b). Blue (red)

lines represent significant negative (positive) correlation at the 95% confidence level. The standardized regression line for 20CR is in green

meridional wind anomalies from the four reanalyses and CMIP5 model mean is shown in Fig. 8. In all four reanalyses, there is a significant negative correlation over Texas, and in the 20CR it exists over much of the Southern Plains, southeastern US, and GOM. The CMIP5 model mean (Fig. 8e) also simulates a significant negative correlation over Texas, but it is weaker than in the reanalyses. The area of strongest negative correlation in the reanalysis and in the models coincides with the placement of the core of the GPLLJ, which is slightly farther east in the CMIP5 model mean (as seen in Fig. 6).

To determine whether simulation of the GPLLJ is affecting the models' ability to capture the accurate ENSO–GPLLJ relationship, the strength and position of the GPLLJ in the five models with the strongest negative DJF ENSO–MAM GPLLJ correlations, labeled the “best spring models” (Fig. 9a), is compared to the five models with the weakest negative DJF ENSO–MAM GPLLJ correlations, labeled the “worst spring models” (Fig. 9b). The selected models are identified in Table 1. Overall, the differences in the GPLLJ between the two categories of models are not large. The worst models have a slightly weaker GPLLJ (peaking at $\sim 2.5 \text{ m s}^{-1}$) than the best models (peaking at $\sim 3 \text{ m s}^{-1}$), and while the worst models place the GPLLJ slightly farther east, this is due to the MIROC-ESM and MIROC-ESM-CHEM models, which place the core of the GPLLJ over the eastern GOM (not shown). Therefore, errors in simulating the intensity and

location of the GPLLJ do not appear to be a major reason for the difficulty for some models to represent the observed ENSO–GPLLJ correlation in the spring.

The analysis of the spatial correlation between DJF ENSO and the following JAS GPLLJ in the reanalyses and CMIP5 model mean is shown in Fig. 10. A significant positive correlation exists over Texas and northeastward to the upper Midwest in both the 20CR (Fig. 10a) and ERA20C (Fig. 10b) and over a much smaller region in the ERA-Interim (Fig. 10c). The CFSR has positive correlations over the Midwest, but none are significant (Fig. 10d). These correlations are shifted north from the spring, consistent with the northward movement of the GPLLJ. The GPLLJ also shifts west from the spring to the summer, which places the strongest positive correlations on the eastern side of the GPLLJ in the summer. This suggests that the GPLLJ is shifted east in summers following an El Niño event. However, the CMIP5 model mean completely lacks this positive correlation anywhere over the Great Plains (Fig. 10e).

Similar to the results found in the spring, the models' inability to simulate the observed ENSO–GPLLJ relationship in the summer does not appear to be due to poor model simulation of the location or intensity of the GPLLJ. The model mean places the core of the GPLLJ near the Texas panhandle (Fig. 10e), is only slightly weaker (peaking at $\sim 5 \text{ m s}^{-1}$) than the reanalyses (peaking at $5.5\text{--}6 \text{ m s}^{-1}$), and from Section 3a, the vast majority

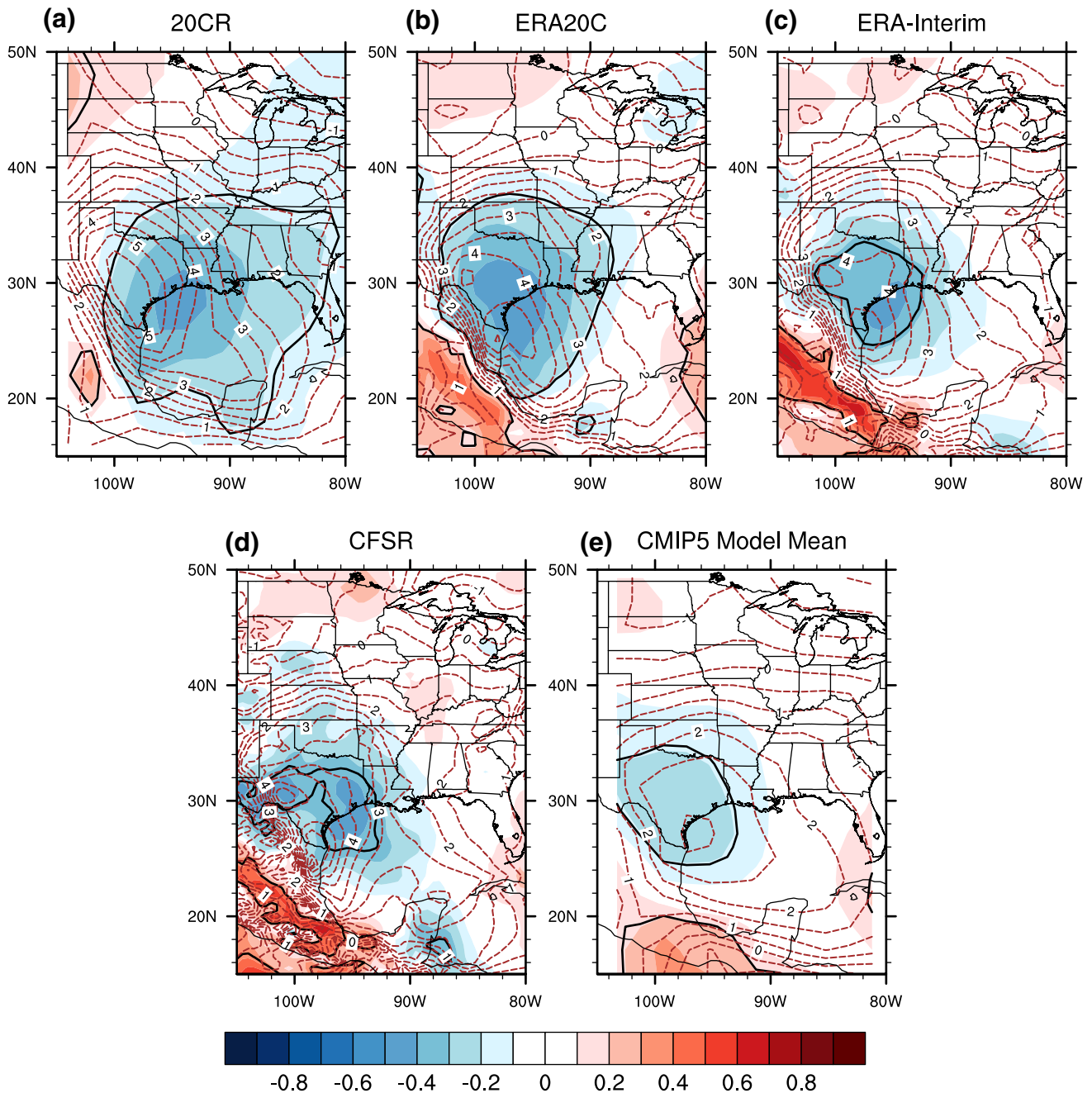


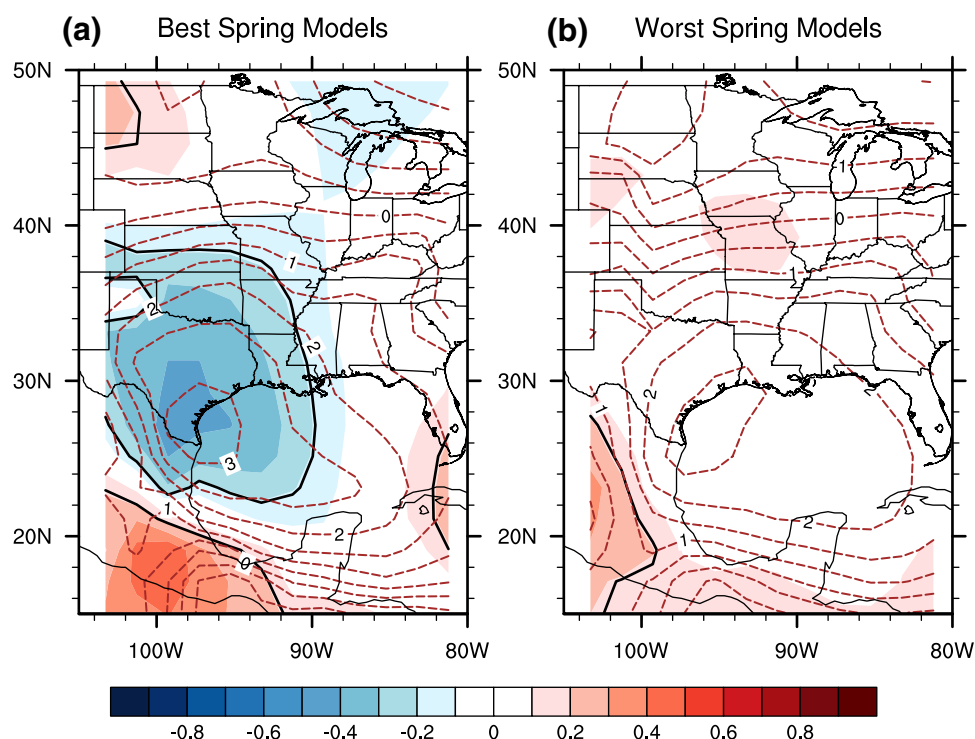
Fig. 8 Cross-correlation between DJF ENSO and 850-hPa meridional wind anomalies in the following MAM (shading), and the mean MAM 850-hPa meridional wind over the period (red dashed contours; contour interval 0.5 m s^{-1}) for 20CR (a), ERA20C (b), ERA-

Interim (c), CFSR (d), and CMIP5 model mean (e). All correlations within the bolded line are statistically significant at the 95% confidence level

of models do not have statistically significant errors in GPLLJ intensity. Differences in the GPLLJ are examined between the five models with the most positive DJF ENSO–JAS GPLLJ correlation, labeled the “best summer models” (Fig. 11a), and the five models with the most negative DJF ENSO–JAS GPLLJ correlation, labeled the “worst summer models” (Fig. 11b). The selected models

are identified in Table 1. The worst models have a weaker GPLLJ (peaking at $\sim 4 \text{ m s}^{-1}$) than the best models (peaking at $\sim 5.5 \text{ m s}^{-1}$), but the location of the GPLLJ is virtually the same in both groups of models. Therefore, it is not likely that a displaced GPLLJ is a major factor in the failure of the models to capture the positive DJF ENSO–JAS GPLLJ correlation seen in the reanalyses.

Fig. 9 Same as Fig. 8, except for the mean of the five models with the strongest negative DJF ENSO–MAM GPLLJ correlation (a), and the mean of the five models with the weakest negative DJF ENSO–MAM GPLLJ correlation (b)



4.3 Effects on GPLLJ characteristics

It is important to examine how ENSO affects the frequency and intensity of individual GPLLJ events, because these are what drive heavy precipitation events. The time of day examined is 06Z, which is when the GPLLJ is strongest (Fig. 5; Higgins et al. 1997; Jiang et al. 2007, Pu and Dickinson 2014). As shown in Table 3, the average 850-hPa meridional wind in ERA-Interim over all days in MAM following DJF La Niñas is significantly stronger (at the 95% confidence level) than it is following DJF El Niños, with the reverse relationship holding for the JAS 850-hPa meridional wind. However, the response of the MAM and JAS meridional wind to neutral ENSO events is less clear, as a significant difference only exists between neutral and El Niño years, not between neutral and La Niña years.

When only including days that have a GPLLJ “event”, defined here as 850-hPa meridional wind that is at least one standard deviation above the mean, there is no statistically significant difference in the strength of the MAM GPLLJ between El Niño and La Niña years or neutral years in ERA-Interim (Table 3). Instead, the influence of ENSO is on the frequency of MAM GPLLJ events, as nearly five more events occur per year on average following DJF La Niña events compared to El Niño events (~37% increase), a difference that is statistically significant. This may be due to La Niña events resulting in more frequent (but not necessarily more intense) high SLP anomalies over the IAS, which Krishnamurthy et al. (2015) found to play a critical role in

the mechanism that drives the relationship between ENSO and the MAM GPLLJ. In JAS, GPLLJ events following DJF El Niños are significantly more frequent (by ~62%) and significantly more intense than GPLLJ events following DJF La Niñas (Table 3). However, in both seasons, the differences in frequency and intensity between years following neutral events and years following El Niño and La Niña events are mostly insignificant, which indicates that the GPLLJ is much less predictable during ENSO-neutral years.

To analyze the spatial distribution of ENSO’s influence on GPLLJ intensity, the difference in MAM meridional wind during GPLLJ events between years following DJF El Niño and La Niña events in ERA-Interim is shown in Fig. 12a. To the northeast of the strongest MAM GPLLJ, the meridional wind is at least $1.8\text{--}2\text{ m s}^{-1}$ stronger following El Niños compared to La Niñas, while to the west of the peak of the GPLLJ over western Texas, the meridional wind is $1\text{--}2\text{ m s}^{-1}$ weaker. This indicates that ENSO is influencing MAM GPLLJ event intensity (stronger GPLLJ following La Niñas than El Niños) northeast of the GPLLJ maxima, but this influence does not extend into the rest of the GPLLJ. The spatial difference in average annual frequency of MAM GPLLJ events between years following DJF El Niño and La Niña (Fig. 12b.) shows two to six more GPLLJ events occur per year following La Niña events than El Niño events over much of Oklahoma and Texas, where the GPLLJ is strongest in MAM. This demonstrates that the effect of ENSO on MAM GPLLJ frequency exists over a much larger area than the effect on MAM GPLLJ intensity.

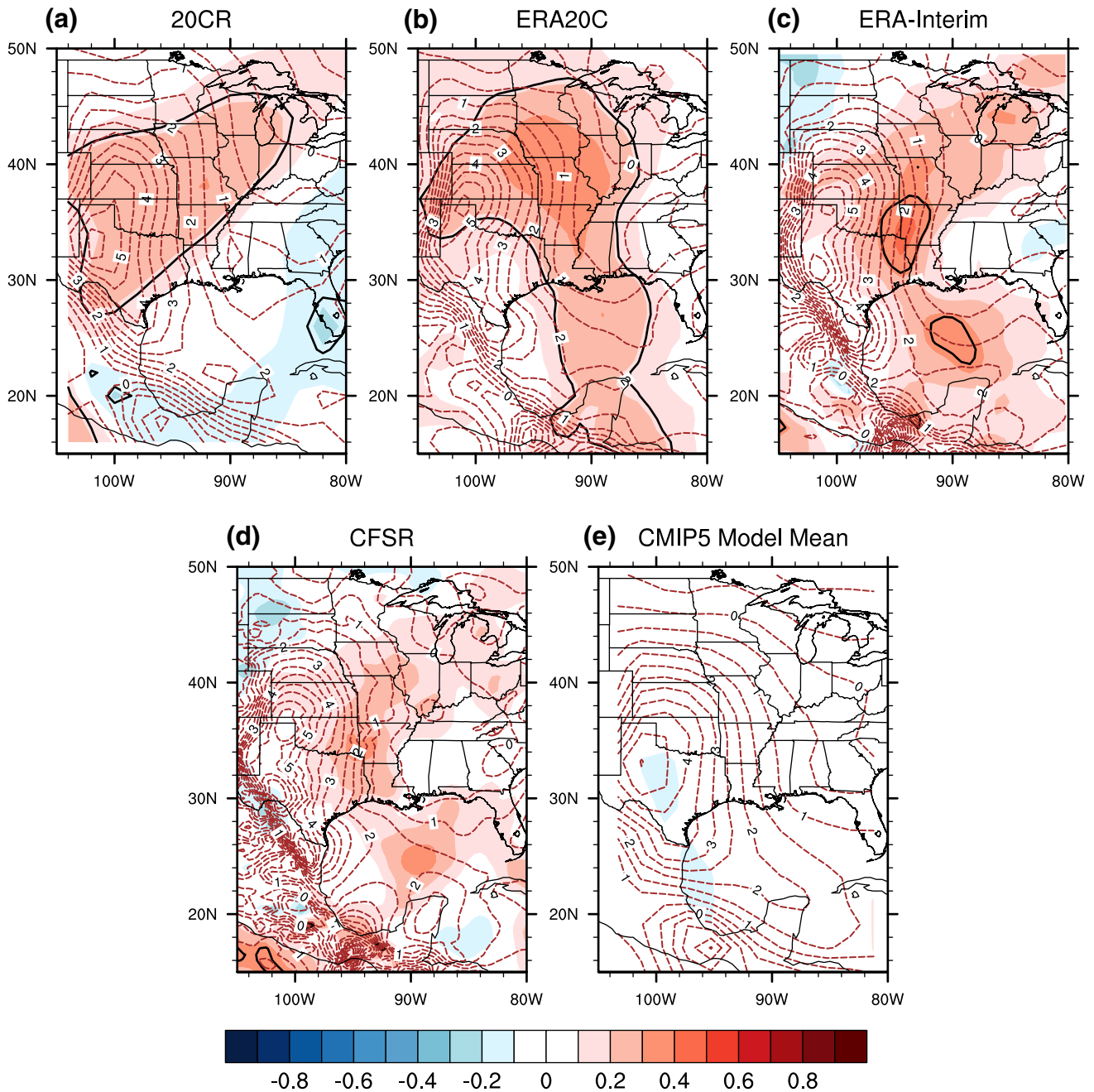


Fig. 10 Same as Fig. 8, except for the JAS 850-hPa meridional wind

The analysis of the effects of ENSO on GPLLJ characteristics is shown in Fig. 13 for JAS. In contrast to MAM, the JAS meridional wind in ERA-Interim during GPLLJ events is clearly affected by ENSO over a large region (Fig. 13a), encompassing eastern Texas, the Texas panhandle, Oklahoma, southeastern Kansas, and central Missouri, where the meridional wind is stronger following DJF El Niño events than DJF La Niña events (by 0.6–1.4 m s⁻¹). The average frequency of JAS GPLLJ events is also

substantially higher following DJF El Niños compared to DJF La Niñas (by 3–8 events per year) over this same area (Fig. 13b). Hence, ENSO has a widespread influence on the frequency and intensity of GPLLJ events over the central US in JAS.

The ability of the CMIP5 models to capture the observed influence of ENSO on the frequency and intensity of GPLLJ events is examined using one ensemble member each from three models (CNRM-CM5,

Fig. 11 Same as Fig. 9, except for the JAS 850-hPa meridional wind, and for the models with the most positive DJF ENSO–JAS GPLLJ correlation (a), and the models with the most negative DJF ENSO–JAS GPLLJ correlation (b)

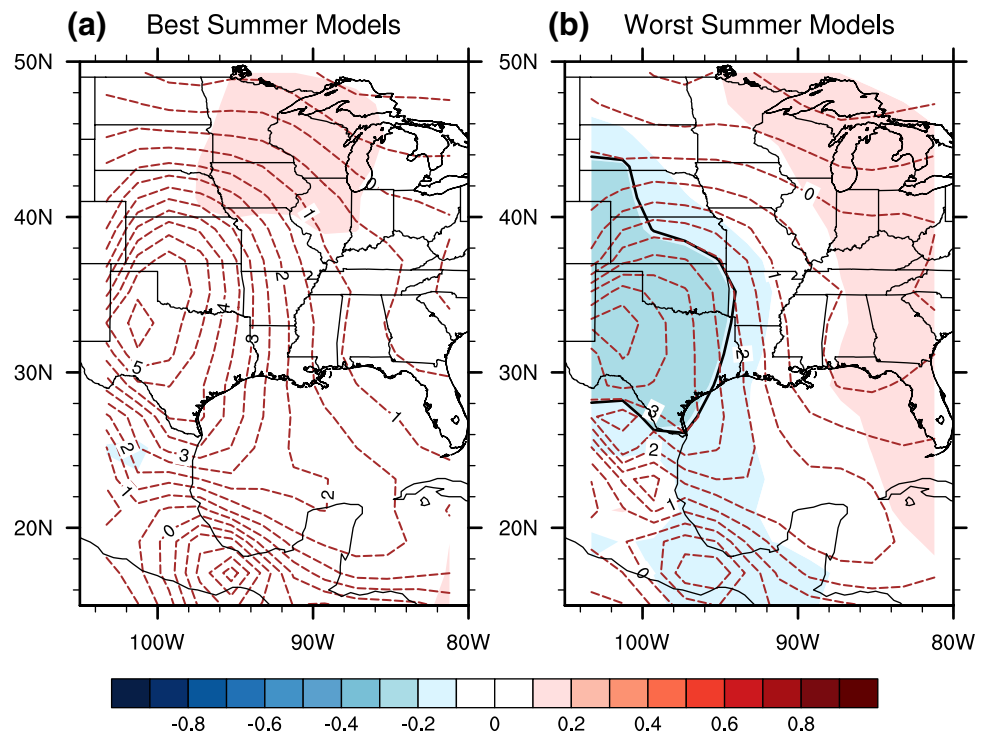


Table 3 Effects of DJF ENSO on the mean daily 850-hPa meridional wind, mean GPLLJ event, and frequency of GPLLJ events in the following MAM and JAS in ERA-Interim

	MAM			JAS		
	El Niño	La Niña	Neutral	El Niño	La Niña	Neutral
Average meridional wind ($m s^{-1}$)	3.76	4.92	4.40	5.80	5.12	5.24
Average GPLLJ event ($m s^{-1}$)	12.92	12.98	12.75	11.80	11.21	11.57
Number of GPLLJ events per year	12.5	17.2	15.6	17.0	10.5	<i>14.0</i>

See text for the definition of a GPLLJ event. Values for El Niño and La Niña events are bolded if the difference between them is statistically significant at the 95% level. Values for neutral events are bolded if they are significantly different from El Niño and italicized if they are significantly different from La Niña

FGOALS-g2, and MIROC-ESM). As shown in Table 4, only the CNRM-CM5 model simulates a significant (at the 95% confidence level) influence on the average MAM 850-hPa meridional wind, with the flow significantly stronger following DJF La Niña events than DJF El Niño events. There is little difference in the mean MAM GPLLJ event strength in this model between El Niño and La Niña years, but the frequency of GPLLJ events increases significantly following La Niñas compared to El Niños (by ~79%), consistent with ERA-Interim (Table 3). In the FGOALS-g2 model, the frequency and intensity of MAM GPLLJ events exhibit no significant change following El Niño and La Niña events, while the MIROC-ESM model does simulate a significant difference in the intensity of the GPLLJ. As expected from results in Sect. 4a, none of the models simulate the observed influence of ENSO on the mean JAS GPLLJ. However, it is necessary to expand these results to additional CMIP5 models.

5 Factors affecting ENSO–GPLLJ relationship in CMIP5

5.1 ENSO SST patterns

As this study has shown, some CMIP5 models struggle to represent the observed DJF ENSO–MAM GPLLJ relationship, and none of them can simulate the observed DJF ENSO – JAS GPLLJ relationship. To determine whether this could be due to a poor simulation of the strength or structure of ENSO, the average DJF SST anomalies during El Niño events in the HadISST1 (Fig. 14a) are compared to the CMIP5 model mean (Fig. 14b). It is apparent that the CMIP5 model mean is mostly able to capture the strength of El Niño events in the equatorial Pacific, though SST anomalies in the north Pacific and the Atlantic are small compared to observations. Also included in Fig. 14 are the SST anomalies in the “best spring models” (Fig. 14c)

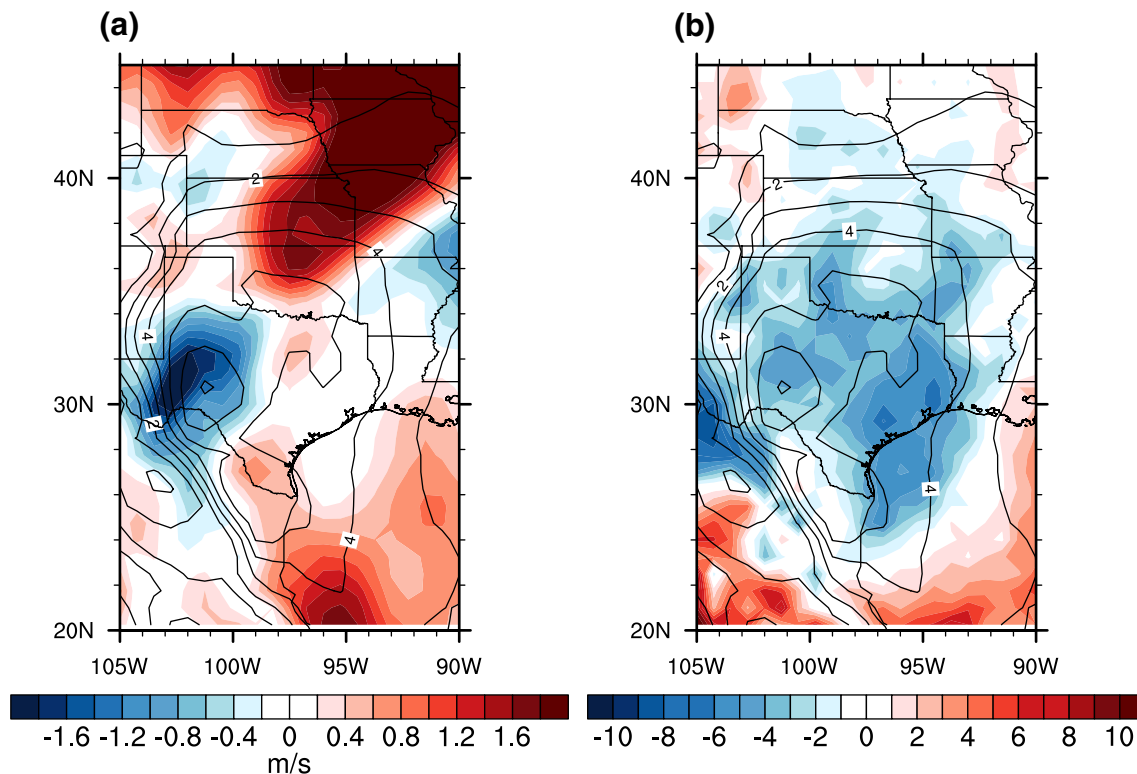


Fig. 12 Difference in MAM meridional wind during GPLLJ events (a) and the difference in average annual frequency of MAM GPLLJ events at each grid point (b) between years following DJF El Niño

and La Niña events in ERA-Interim. See text for the definition of a GPLLJ event. The mean MAM meridional wind is plotted as black contours (contour interval 1 m s^{-1})

and “worst spring models” (Fig. 14d; see Sect. 4b for definitions). The worst models have El Niño events that are too weak (by $\sim 0.8 \text{ }^\circ\text{C}$) compared to observations, while El Niño events in the best models are approximately $0.4 \text{ }^\circ\text{C}$ stronger than observations. Similar results are found for La Niña events (not shown).

Since the SST pattern associated with ENSO is weaker in the worst models, we hypothesize that its effects on the overall atmospheric circulation, and thus on the mechanisms that drive the GPLLJ in MAM, are lessened as well. ENSO SST patterns were examined in the “best summer models” and “worst summer models”, but in contrast to the spring, the worst models in the summer do not simulate a weaker ENSO SST pattern than the best models (not shown). As even the best CMIP5 models fail to capture the significant positive correlation between ENSO and the summer GPLLJ, we cannot draw conclusions based on this “best” and “worst” model grouping.

5.2 Atmospheric response to ENSO

If CMIP5 models are unable to represent the atmospheric response to ENSO, they will not be capable of capturing the observed effects of ENSO on the GPLLJ. Polade et al.

(2013) and Hurwitz et al. (2014) have shown that CMIP5 models reproduce the observed Pacific and upper tropospheric responses to ENSO in boreal autumn and winter, including the corresponding North American winter precipitation. However, the impact on mechanisms driving the GPLLJ response in MAM and JAS has not yet been examined.

The influence of ENSO on MAM 850-hPa geopotential heights is examined in Fig. 15. From reanalyses, DJF ENSO is shown to be negatively correlated with MAM 850-hPa geopotential heights over the eastern Pacific and western Atlantic and positively correlated in the western Pacific, agreeing with previous studies (Shinker and Bartlein 2009). The CMIP5 model mean (Fig. 15d) and “best spring models” (Fig. 15e) are successful at representing this relationship, while the “worst spring models” simulate the observed pattern but it is too weak (Fig. 15f). This gives further evidence to the hypothesis that these models are struggling to represent the correct ENSO–GPLLJ relationship in the spring because they are simulating ENSO that is too weak, and thus it is not having enough influence on geopotential heights which are one of the most important large-scale drivers of GPLLJ variability.

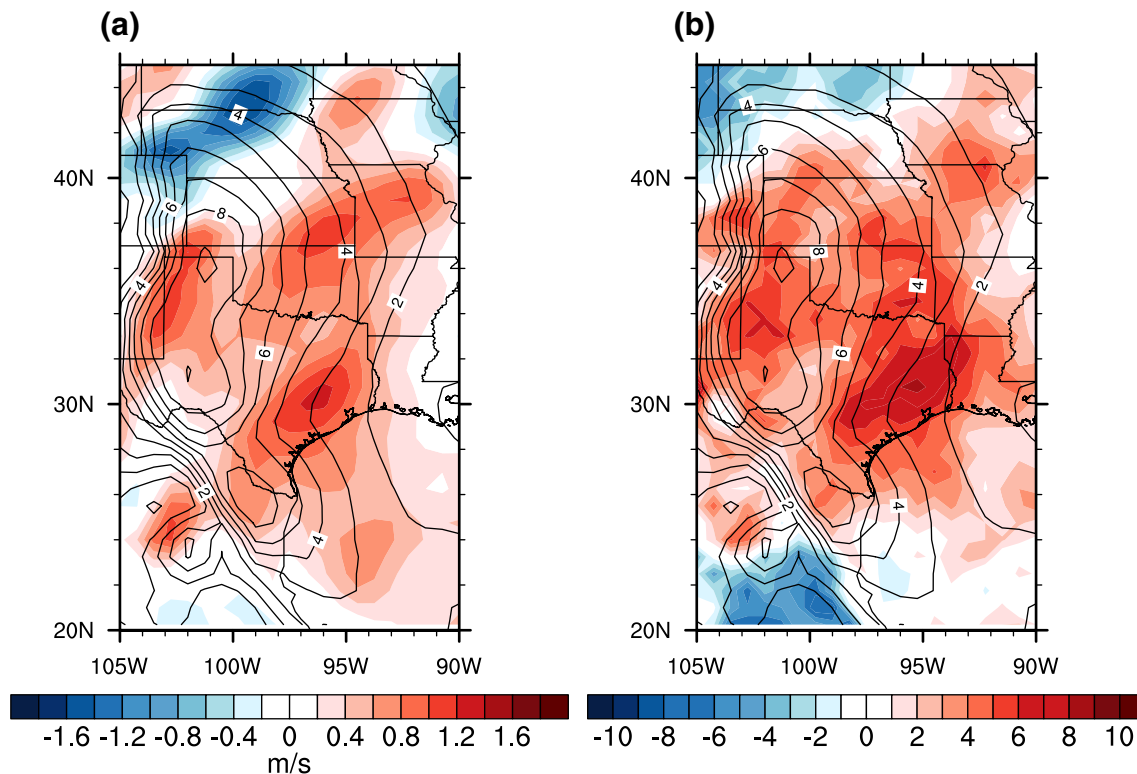


Fig. 13 Same as Fig. 12, but for the JAS meridional wind

The correlation between DJF ENSO and the following JAS 850-hPa geopotential heights is also shown in Fig. 16. A negative correlation is observed in the northern and western US, while a positive correlation is observed in the southeastern US creating a strong height gradient across the Great Plains (e.g. Harding and Snyder 2015). However, the CMIP5 model mean is mostly unable to simulate this gradient associated with ENSO, as it exhibits a small (but insignificant) positive correlation across the eastern and western US (Fig. 16d). The “worst summer models” do a particularly poor job because they simulate a significant positive correlation over the western US (Fig. 16f), hence reversing the observed geopotential height gradient. The correlation between DJF ENSO and JAS 850-hPa geopotential heights is shown in Fig. 16e for the model that simulates the most positive (closest to observed) DJF ENSO–JAS GPLLJ correlation (CMCC-CMS), though it is still not significant. It is apparent that this model is more successful in comparison to the model mean, as it simulates the height gradient across the US that is seen in the reanalyses. Therefore, it appears that the models’ inability to simulate the positive DJF ENSO–JAS GPLLJ relationship seen in observations can be at least partially attributed to an inaccurate representation of the effects of ENSO on geopotential heights in the following summer across the US.

6 Discussion and conclusions

Based on the results from this study using historical CMIP5 simulations and multiple reanalyses, a nocturnal GPLLJ exists in CMIP5 models, and some overall features of the GPLLJ in the models are comparable to the reanalyses. However, several important details differ. One of the most striking errors is the models’ underestimation of the strength of the GPLLJ in the spring. The MAM model mean GPLLJ is significantly weaker than the 20CR, and a majority of models (25 out of 42) simulate a MAM GPLLJ that is significantly weaker. However, the models perform much better in JAS. In addition to strength, the location and timing of the GPLLJ in the CMIP5 models differ from the reanalyses in a number of ways. In the models, the core of the GPLLJ is located at a lower level, and the peak of the GPLLJ too late in the summer, agreeing with the findings from Sheffield et al. (2013) using a limited number of models. The GPLLJ in the models is also located farther east than it is in the reanalyses.

Many of these errors in location and timing of the GPLLJ also existed in simulations from phase 3 of the Coupled Model Intercomparison Project (CMIP3) (Cook et al. 2008), so there have not been substantial improvements in GPLLJ simulation between the two generations of climate models. These errors could be having a considerable negative impact

Table 4 Same as Table 3, but for three CMIP5 models and for just El Niño/La Niña events

	MAM						JAS					
	CNRM-CM5		FGOALS-g2		MIROC-ESM		CNRM-CM5		FGOALS-g2		MIROC-ESM	
	El Niño	La Niña	El Niño	La Niña	El Niño	La Niña	El Niño	La Niña	El Niño	La Niña	El Niño	La Niña
Average meridional wind ($m s^{-1}$)	2.81	4.52	2.11	2.41	3.04	3.04	5.90	5.95	4.52	4.50	5.92	5.68
Average GPLLJ event ($m s^{-1}$)	12.44	12.18	9.62	9.75	10.79	11.26	11.59	11.69	10.17	10.07	12.84	13.15
Number of GPLLJ events per year	9.9	17.7	14.8	14.8	15.7	16.1	14.0	13.3	15.8	15.8	16.9	15.5

on the models’ ability to accurately predict heavy rainfall and severe weather events in the central US. When the climatological GPLLJ in the models is poorly simulated, it is likely that the models will be unable to fully capture the extent of its influence on precipitation and severe weather over the Great Plains.

It is also important to note that reanalyses themselves can have biases in comparison to “true” observations. As shown by Berg et al. (2015), ERA-Interim and CFSR contain biases in the GPLLJ compared to observations. The reanalyses overestimate the wind speed and place the core of the GPLLJ at a higher altitude. These biases indicate that two of the CMIP5 biases, placing the GPLLJ too low and simulating a GPLLJ that is too weak, may be overestimated. Using the height of maximum wind in the models (925 hPa) instead of in the reanalyses (850 hPa) identifies a model mean GPLLJ that is stronger, though it is still weaker than the reanalysis mean for all months of the year outside of JAS.

As expected from prior work, ENSO has a substantial impact on the strength of the GPLLJ, with a significant negative correlation in the spring and a significant positive correlation in the summer (Schubert et al. 2004; Weaver et al. 2009; Muñoz and Enfield 2011; Krishnamurthy et al. 2015). The majority of CMIP5 ensemble members (82 out of 131) capture the significant negative DJF ENSO–MAM GPLLJ correlation, and the models and reanalyses generally agree on the placement of this correlation over the core of the GPLLJ. However, in contrast to the reanalyses, the model mean DJF ENSO–JAS GPLLJ correlation is weakly negative, and only two out of 131 ensemble members capture the observed significant positive correlation. With the vast majority of models unable to represent the observed influence of ENSO on the GPLLJ in the summer, the accuracy of their near- and long-term predictions and projections of GPLLJ variability can be questioned.

It is shown that the inability of the CMIP5 models to simulate the influence of ENSO on the GPLLJ is due to simulating ENSO SST patterns that are too weak, which makes the atmospheric response to ENSO too weak, rather than due to simulation of the intensity and location of the GPLLJ. In spring, the atmospheric response to La Niña includes the high geopotential height anomalies over the GOM and Caribbean Sea, which play a crucial role in the mechanism that drives the correlation between ENSO and the GPLLJ in the spring (Krishnamurthy et al. 2015). In the summer, on the other hand, the failure of nearly all the CMIP5 models to reproduce the observed influence of ENSO on the GPLLJ can be attributed to a very poor representation of the impact of DJF ENSO on the 850-hPa geopotential height gradient across the US in the following JAS.

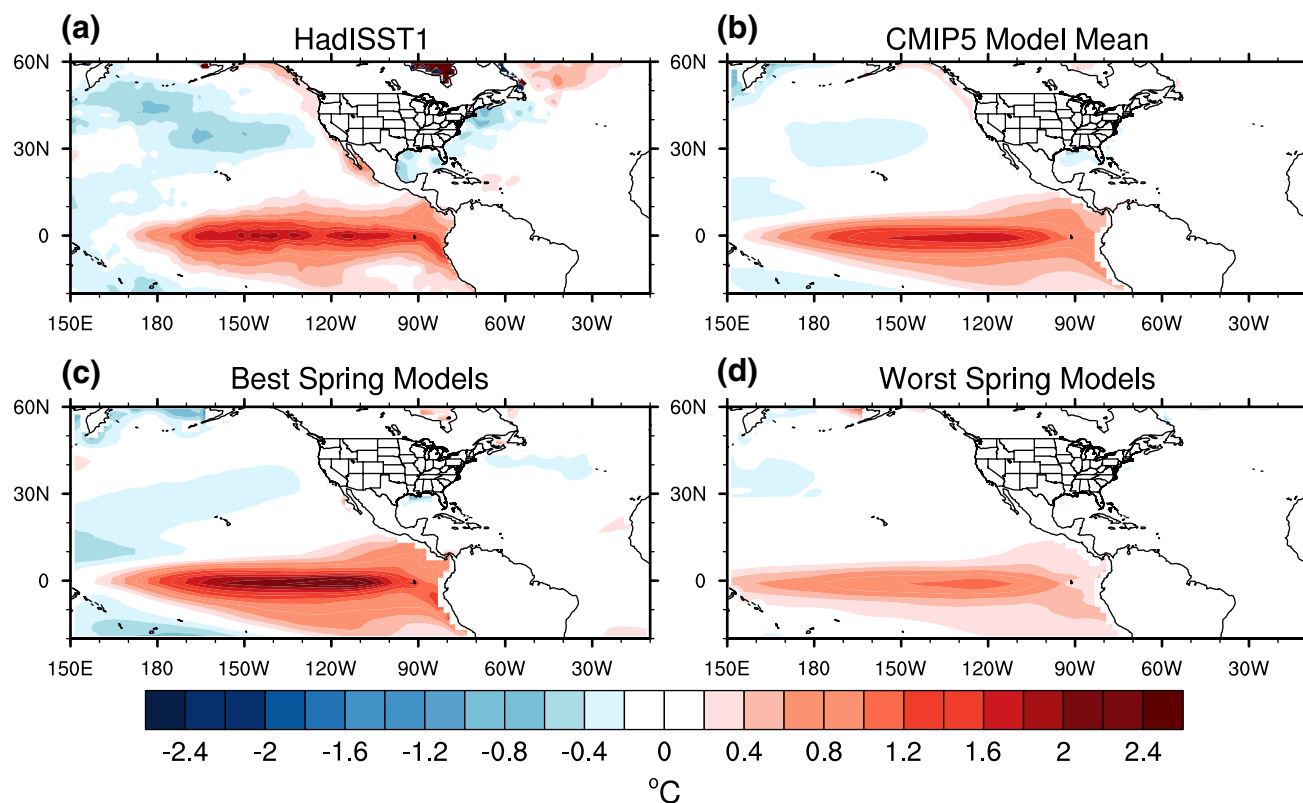


Fig. 14 Mean DJF SST anomalies during DJF El Niño for the HadISST1 (a), CMIP5 model mean (b), “best spring models” (c), and “worst spring models” (d)

These results indicate that predictions and projections of the variability of the GPLLJ associated with El Niño and La Niña events could be greatly improved in future generations of climate models if models are able to simulate stronger (more realistic) SST patterns, and more accurately represent the summertime atmospheric response to ENSO events across the US. Predictability during neutral ENSO events is not as clearly evident in the reanalysis. While the ENSO SST magnitude is highlighted by this study, other ENSO biases in the CMIP5 models such as a narrow bias in meridional width (Zhang and Jin 2012) and ENSO variability and inaccurate phase locking (e.g. Krishnamurthy et al. 2015) could be influencing the relationship with the GPLLJ. Prior studies have not found significant improvements from CMIP3 to CMIP5 models in their representation of ENSO (Bellenger et al. 2014), which could partly explain why GPLLJ simulation has not greatly improved.

In ERA-Interim the statistically significant effect of ENSO is on the frequency, not intensity, of GPLLJ events in the spring, while both frequency and intensity are significantly affected in the summer. Since ENSO affects the frequency, not intensity, of MAM GPLLJ events, it is likely

that DJF La Niñas (El Niños) will result in more (less) frequent heavy rainfall and severe weather events in the spring across the Central US, but they will not necessarily be more intense. In the summer, however, both the frequency and intensity of heavy rainfall and severe weather events will likely increase (decrease) following DJF El Niños (La Niñas). The effect of ENSO on GPLLJ characteristics was examined in three CMIP5 models (CNRM-CM5, FGOALS-g2, and MIROC-ESM), and it was discovered that only the CNRM-CM5 model can capture the accurate influence (e.g. significantly more frequent, but not more intense, GPLLJ events following La Niñas) in the spring. None of the models simulate the observed impact of ENSO on GPLLJ characteristics in the summer.

Reanalyses (including the ERA-Interim and CFSR) underestimate the frequency of GPLLJ events, particularly strong GPLLJ events (Berg et al. 2015). This is especially prevalent among the reanalyses with coarser resolutions (e.g. ERA-Interim). The 20CR and ERA20C, along with many of the CMIP5 models, have even lower resolutions than the ERA-Interim, which could be limiting their ability to accurately depict various features of the GPLLJ. Errors in the CMIP5 simulations may be arising through

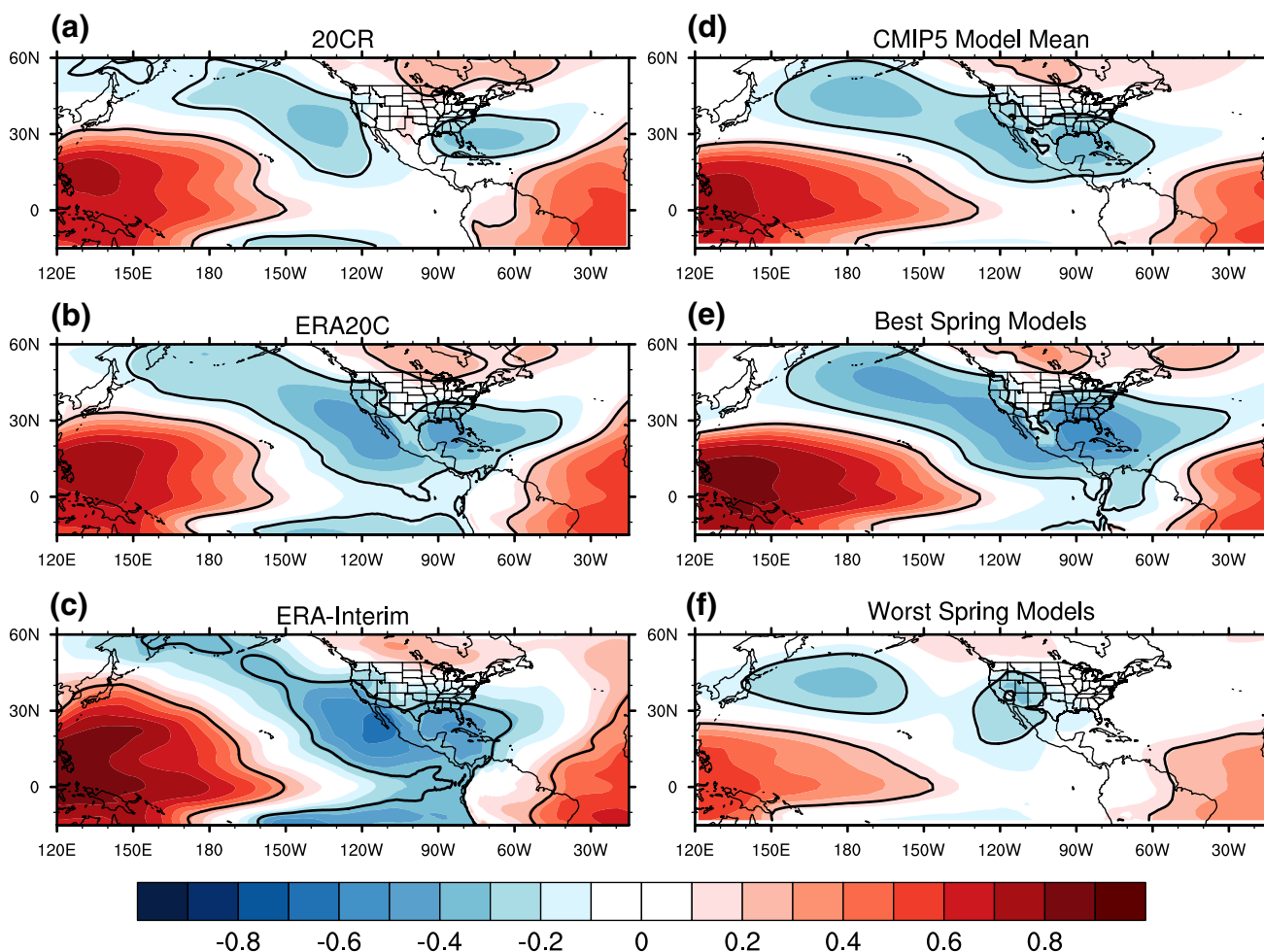


Fig. 15 Lagged correlation between MAM 850-hPa geopotential height anomalies and the previous DJF ENSO in 20CR (a), ERA20C (b), ERA-Interim (c), CMIP5 model mean (d), “best spring models”

(e), and “worst spring models” (f). All correlations within the bolded line are statistically significant at the 95% confidence level using a two-tailed probability test

poor representation of topographical features which could be inhibiting the models’ ability to simulate orographic mechanisms of the GPLLJ (e.g. Wexler 1961; Holton 1967). The questions regarding the accuracy of reanalyses and CMIP5 simulations highlight the need to increase the coverage and availability of wind observations across the Great Plains.

While this study focused on the role of ENSO in driving the variability of the GPLLJ, it is known from previous studies that other teleconnections are important as well. These include the enhancement of the GPLLJ by a negative phase of the Pacific–North American teleconnection pattern (Harding and Snyder 2015), a significant negative correlation between the Pacific Decadal Oscillation and the GPLLJ in the spring (Muñoz and Enfield 2011), and a link between GPLLJ variability and the North Atlantic Oscillation in the summer (Weaver and Nigam 2008). Future work

is needed to understand the influence and interconnectivity of these teleconnections on GPLLJ variability, and the ENSO–GPLLJ relationship in observations and climate model simulations.

This study further developed our understanding of the relationship between the GPLLJ and ENSO, in reanalyses and CMIP5 models. Simulation ability can be attributed to the representation of the strength of ENSO and its impacts on the atmospheric circulation in the models. If simulation ability can be improved, through enhanced resolution, improved ocean–atmosphere coupling, representation of heating from convection, or other mechanisms, our ability to accurately predict and project the variability of the GPLLJ, and thus precipitation and severe weather over the Great Plains, will be enhanced.

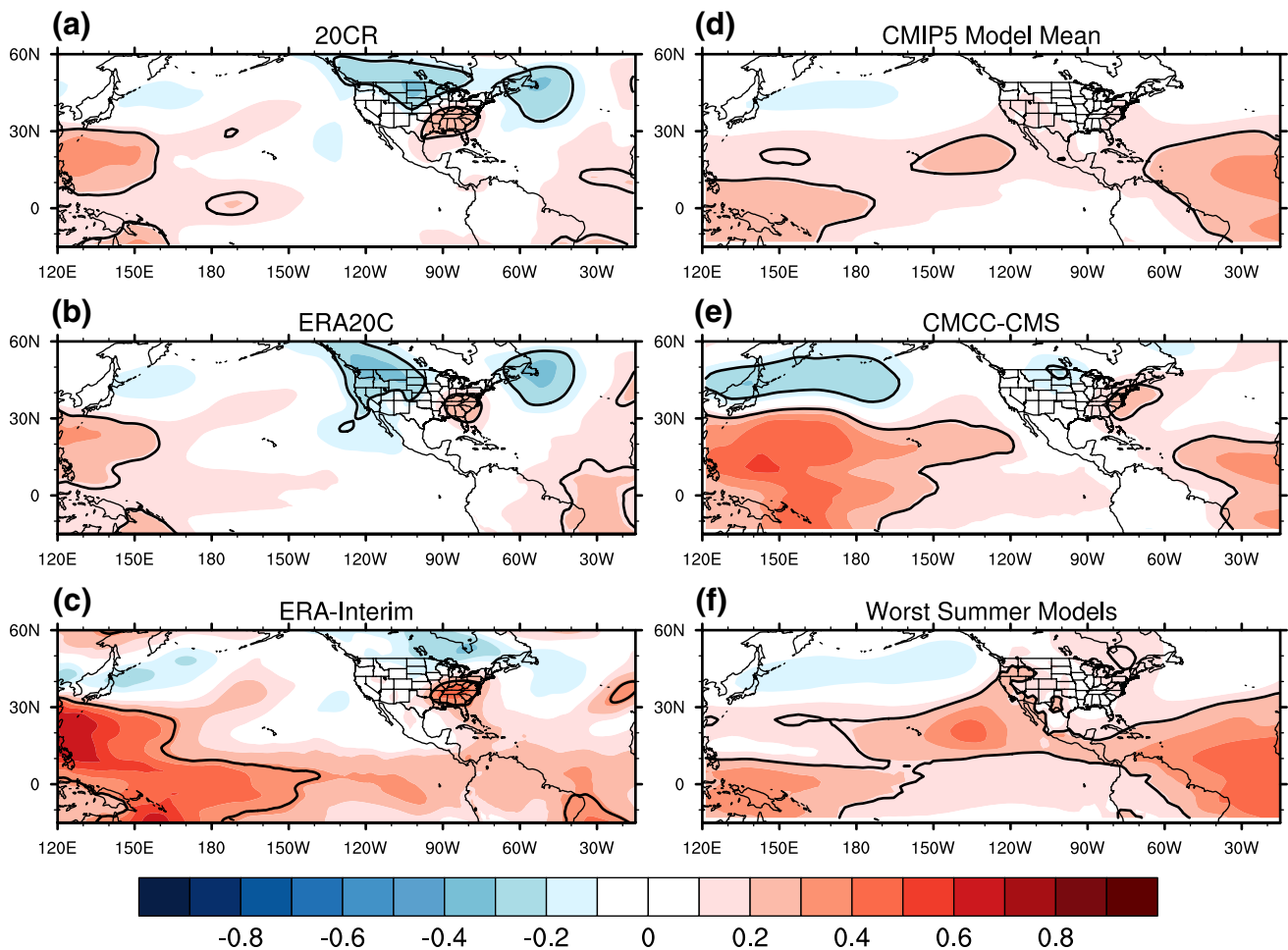


Fig. 16 Same as Fig. 15, but for JAS 850-hPa geopotential height anomalies

Acknowledgements The authors thank the anonymous reviewer for thoughtful comments and suggestions that greatly strengthened the manuscript. We acknowledge the World Climate Research Programme's Working Group on Coupled Modelling, which is responsible for CMIP5, and thank the climate modeling groups for producing and making available their model output. For CMIP5, the US Department of Energy's Program for Climate Model Diagnosis and Intercomparison provides coordinating support and led development of software infrastructure in partnership with the Global Organization for Earth System Science Portals. Support for the Twentieth Century Reanalysis Project version 2c dataset is provided by the US Department of Energy, Office of Science Biological and Environmental Research (BER), and by the National Oceanic and Atmospheric Administration Climate Program Office. ERA20C and ERA-Interim data is provided courtesy of ECMWF, and CFSR data is carried out by the Environmental Modeling Center (EMC), National Centers for Environmental Prediction (NCEP). We also acknowledge the Met Office Hadley Centre for providing HadISST1 data.

References

- Adachi Y et al (2013) Basic performance of a new earth system model of the Meteorological Research Institute (MRI-ESM1). *Pap Meteorol Geophys* 64:1–19. doi:[10.2467/mripapers.64.1](https://doi.org/10.2467/mripapers.64.1)
- Arora VK et al (2011) Carbon emission limits required to satisfy future representative concentration pathways of greenhouse gases. *Geophys Res Lett* 38:L05805. doi:[10.1029/2010GL046270](https://doi.org/10.1029/2010GL046270)
- Baek H-J et al (2013) Climate change in the 21st century simulated by HadGEM2-AO under representative concentration pathways. *Asia-Pac J Atmos Sci* 49:603–618. doi:[10.1007/s13143-013-0053-7](https://doi.org/10.1007/s13143-013-0053-7)
- Bao Q et al (2012) The flexible global ocean–atmosphere–land system model, spectral version 2: FGOALS-s2. *Adv Atmos Sci* 30:561–576. doi:[10.1007/s00376-012-2113-9](https://doi.org/10.1007/s00376-012-2113-9)
- Barandiaran D, Wang SY, Hilburn K (2013) Observed trends in the Great Plains low-level jet and associated precipitation changes in relation to recent droughts. *Geophys Res Lett* 40:6247–6251. doi:[10.1002/2013GL058296](https://doi.org/10.1002/2013GL058296)
- Bellenger H, Guilyardi E, Leloup J, Lengaigne M, Vialard J (2014) ENSO representation in climate models: from CMIP3 to CMIP5. *Clim Dyn* 42:1999–2018. doi:[10.1007/s00382-013-1783-z](https://doi.org/10.1007/s00382-013-1783-z)
- Bentsen M et al (2013) The Norwegian Earth System Model, NorESM1-M—part 1: description and basic evaluation of the physical climate. *Geosci Model Dev* 6:687–720. doi:[10.5194/gmd-6-687-2013](https://doi.org/10.5194/gmd-6-687-2013)
- Berg LK, Riihimaki LD, Qian Y, Yan H, Huang M (2015) The low-level jet over the southern Great Plains determined from observations and reanalyses and its impact on moisture transport. *J Clim* 28:6682–6706. doi:[10.1175/JCLI-D-14-00719.1](https://doi.org/10.1175/JCLI-D-14-00719.1)

- Blackadar AK (1957) Boundary layer wind maxima and their significance for the growth of nocturnal inversions. *Bull Am Meteorol Soc* 38:283–290
- Collins M, Tett SFB, Cooper C (2001) The internal climate variability of HadCM3, a version of the Hadley centre coupled model without flux adjustments. *Clim Dyn* 17:61–81. doi:10.1007/s003820000094
- Compo GP et al (2011) The twentieth century reanalysis project. *Q J R Meteorol Soc* 137(654):1–28. doi:10.1002/qj.776
- Cook KH, Vizy EK (2010) Hydrodynamics of the Caribbean low-level jet and its relationship to precipitation. *J Clim* 23:1477–1494. doi:10.1175/2009JCLI3210.1
- Cook KH, Vizy EK, Launer ZS, Patricola CM (2008) Springtime intensification of the Great Plains low-level jet and Midwest precipitation in GCM simulations of the twenty-first century. *J Clim* 21:6321–6340. doi:10.1175/2008JCLI2355.1
- Delworth TL et al (2006) GFDL's CM2 global coupled climate models. Part I: formulation and simulation characteristics. *J Clim* 19:643–674. doi:10.1175/JCLI3629.1
- Donner LJ et al (2011) The dynamical core, physical parameterizations, and basic simulation characteristics of the atmospheric component AM3 of the GFDL global coupled model CM3. *J Clim* 24:3484–3519. doi:10.1175/2011JCLI3955.1
- Dufresne J-L, Coauthors (2013) Climate change projections using the IPSL-CM5 earth system model: from CMIP3 to CMIP5. *Clim Dyn* 40:2123–2165. doi:10.1007/s00382-012-1636-1
- Eichler T, Higgins W (2006) Climatology and ENSO-related variability of North American extratropical cyclone activity. *J Clim* 19:2076–2093. doi:10.1175/JCLI3725.1
- Gent PR et al (2011) The community climate system model version 4. *J Clim* 24:4973–4991. doi:10.1175/2011JCLI4083.1
- Harding KJ, Snyder PK (2015) The relationship between the Pacific–North American teleconnection pattern, the Great Plains low-level jet, and North Central US heavy rainfall events. *J Clim* 28:6729–6742. doi:10.1175/JCLI-D-14-00657.1
- Higgins RW, Yao Y, Yarosh ES, Janowiak JE, Mo KC (1997) Influence of the Great Plains low-level jet on summertime precipitation and moisture transport over the central United States. *J Clim* 10:481–507. doi:10.1175/1520-0442(1997)010<0481:IOTGPL>2.0.CO;2
- Holton JR (1967) The diurnal boundary layer wind oscillation above sloping terrain. *Tellus* 19:199–205
- Hurwitz MM, Calvo N, Garfinkel CI, Butler AH, Ineson S, Cagnazzo C, Manzini E, Peña-Ortiz C (2014) Extra-tropical atmospheric response to ENSO in the CMIP5 models. *Clim Dyn* 43:3367–3376. doi:10.1007/s00382-014-2110-z
- Jiang X, Lau N-C, Held IM, Ploshay JJ (2007) Mechanisms of the Great Plains low-level jet as simulated in an AGCM. *J Atmos Sci* 64:532–547. doi:10.1175/JAS3847.1
- Jones CD et al (2011) The HadGEM2-ES implementation of CMIP5 centennial simulations. *Geosci Model Dev* 4:543–570. doi:10.5194/gmd-4-543-2011
- Kim ST, Yu J-Y (2012) The two types of ENSO in CMIP5 models. *Geophys Res Lett* 39:L11704. doi:10.1029/2012GL052006
- Kim D, Sobel AH, Del Genio AD, Chen Y, Camargo SJ, Yao M-S, Kelley M, Nazarenko L (2012) The tropical subseasonal variability simulated in the NASA GISS general circulation model. *J Clim* 25:4641–4659. doi:10.1175/JCLI-D-11-00447.1
- Krishnamurthy L, Vecchi GA, Msadek R, Wittenberg A, Delworth TL, Zeng F (2015) The seasonality of the Great Plains low-level jet and ENSO relationship. *J Clim* 28:4525–4544. doi:10.1175/JCLI-D-14-00590.1
- Lee SK, Atlas R, Enfield D, Wang C, Liu H (2013) Is there an optimal ENSO pattern that enhances large-scale atmospheric processes conducive to tornado outbreaks in the United States? *J Clim* 26:1626–1642. doi:10.1175/JCLI-D-12-00128.1
- Li L et al (2013) The flexible global ocean–atmosphere–land system model, grid-point version 2: FGOALS-g2. *Adv Atmos Sci* 30:543–560. doi:10.1007/s00376-012-2140-6
- Long MC, Lindsay K, Peacock S, Moore JK, Doney SC (2013) Twentieth-century oceanic carbon uptake and storage in CESM1 (BGC). *J Clim* 26:6775–6800. doi:10.1175/JCLI-D-12-00184.1
- Marsh DR, Mills MJ, Kinnison DE, Lamarque J-F, Calvo N, Polvani LM (2013) Climate change from 1850 to 2005 simulated in CESM1(WACCM). *J Clim* 26:7372–7391. doi:10.1175/JCLI-D-12-00558.1
- Martin ER, Schumacher C (2011) The Caribbean low-level jet and its relationship with precipitation in IPCC AR4 models. *J Clim* 24:5935–5950. doi:10.1175/JCLI-D-11-00134.1
- Meehl GA et al (2013) Climate change projections in CESM1(CAM5) compared to CCSM4. *J Clim* 26:6287–6308. doi:10.1175/JCLI-D-12-00572.1
- Muñoz E, Enfield D (2011) The boreal spring variability of the Intra-Americas low-level jet and its relation with precipitation and tornadoes in the eastern United States. *Clim Dyn* 36:247–259. doi:10.1007/s00382-009-0688-3
- Perez J, Menendez M, Mendez FJ, Losada IJ (2014) Evaluating the performance of CMIP3 and CMIP5 global climate models over the north-east Atlantic region. *Clim Dyn* 43:2663–2680. doi:10.1007/s00382-014-2078-8
- Phipps SJ, Rotstajn LD, Gordon HB, Roberts JL, Hirst AC, Budd WF (2011) The CSIRO Mk3L climate system model version 1.0—part 1: description and evaluation. *Geosci Model Dev* 4:483–509. doi:10.5194/gmd-4-483-2011
- Polade SD, Gershunov A, Cayan DR, Dettinger MD, Pierce DW (2013) Natural climate variability and teleconnections to precipitation over the Pacific–North American region in CMIP3 and CMIP5 models. *Geophys Res Lett* 40:2296–2301. doi:10.1002/grl.50491
- Poli P et al (2016) ERA-20C: an atmospheric reanalysis of the twentieth century. *J Clim* 29:4083–4097. doi:10.1175/JCLI-D-15-0556.1
- Pu B, Dickinson RE (2014) Diurnal spatial variability of Great Plains summer precipitation related to the dynamics of the low-level jet. *J Atmos Sci* 71:1807–1817. doi:10.1175/JAS-D-13-0243.1
- Rayner NA, Parker DE, Horton EB, Folland CK, Alexander LV, Rowell DP, Kent EC, Kaplan A (2003) Global analyses of sea surface temperature, sea ice, and night marine air temperature since the late nineteenth century. *J Geophys Res* 108(D14):4407. doi:10.1029/2002JD002670
- Saha S, Coauthors (2010) The NCEP climate forecast system reanalysis. *Bull Am Meteorol Soc* 91:1015–1057. doi:10.1175/2010BAMS3001.1
- Schubert SM, Suarez J, Pegion PJ, Koster RD, Bacmeister JT (2004) Causes of long-term drought in the U.S. Great Plains. *J Clim* 17:485–503. doi:10.1175/1520-0442(2004)017<0485:COLDIT>2.0.CO;2
- Sheffield J et al (2013) North American climate in CMIP5 experiments. Part I: evaluation of historical simulations of continental and regional climatology. *J Clim* 26:9209–9245. doi:10.1175/JCLI-D-12-00592.1
- Shinker JJ, Bartlein PJ (2009) Visualizing the large-scale patterns of ENSO-related climate anomalies in North America. *Earth Interact* 13(3):1–50. doi:10.1175/2008EI244.1
- Simmons AJ, Poli P, Dee DP, Berrisford P, Hersbach H, Kobayashi S, Peubey C (2014) Estimating low-frequency variability and trends in atmospheric temperature using ERA-Interim. *Q J R Meteorol Soc* 140(679):329–353. doi:10.1002/qj.2317
- Stensrud DJ (1996) Importance of low-level jets to climate: a review. *J Clim* 9:1698–1711. doi:10.1175/1520-0442(1996)009<1698:IOLLJT>2.0.CO;2
- Taylor KE, Stouffer RJ, Meehl GA (2012) An overview of CMIP5 and the experiment design. *Bull Am Meteorol Soc* 93:485–498. doi:10.1175/BAMS-D-11-00094.1

- Voltaire A et al (2013) The CNRM-CM5.1 global climate model: description and basic evaluation. *Clim Dyn* 40:2091–2121. doi:[10.1007/s00382-011-1259-y](https://doi.org/10.1007/s00382-011-1259-y)
- Volodin EM, Diansky NA, Gusev AV (2010) Simulating present-day climate with the INMCM4.0 coupled model of the atmospheric and oceanic general circulations. *Inv Atmos Ocean Phys* 46:414–431. doi:[10.1134/S000143381004002X](https://doi.org/10.1134/S000143381004002X)
- Watanabe M et al (2010) Improved climate simulation by MIROC5: mean states, variability, and climate sensitivity. *J Clim* 23:6312–6335. doi:[10.1175/2010JCLI3679.1](https://doi.org/10.1175/2010JCLI3679.1)
- Weaver SJ, Nigam S (2008) Variability of the Great Plains low-level jet: large-scale circulation context and hydroclimate impacts. *J Clim* 21:1532–1551. doi:[10.1175/2007JCLI1586.1](https://doi.org/10.1175/2007JCLI1586.1)
- Weaver SJ, Schubert S, Wang H (2009) Warm season variations in the low-level circulation and precipitation over the central United States in observations, AMIP simulations, and idealized SST experiments. *J Clim* 22:5401–5420. doi:[10.1175/2009JCLI2984.1](https://doi.org/10.1175/2009JCLI2984.1)
- Wexler H (1961) A boundary layer interpretation of the low level jet. *Tellus* 13:368–378
- Xin X, Wu T, Zhang J (2012) Introductions to the CMIP5 simulations conducted by the BCC climate system model. *Adv Climate Change Res* 8:378–382 (in Chinese)
- Yukimoto S et al (2012) A new global climate model of the Meteorological Research Institute: MRI-CGCM3—model description and basic performance. *J Meteorol Soc Jpn* 90A:23–64. doi:[10.2151/jmsj.2012-A02](https://doi.org/10.2151/jmsj.2012-A02)
- Zanchettin D, Rubino A, Matei D, Bothe O, Jungclaus JH (2013) Multi-decadal-to-centennial SST variability in the MPI-ESM simulation ensemble for the last millennium. *Clim Dyn* 40:1301–1318. doi:[10.1007/s00382-012-1361-9](https://doi.org/10.1007/s00382-012-1361-9)
- Zhang W, Jin F-F (2012) Improvements in the CMIP5 simulations of ENSO-SSTA meridional width. *Geophys Res Lett* 39:L23704. doi:[10.1029/2012GL053588](https://doi.org/10.1029/2012GL053588)
- Zhang T, Sun D-Z (2014) ENSO asymmetry in CMIP5 models. *J Clim* 27:4070–4093. doi:[10.1175/JCLI-D-13-00454.1](https://doi.org/10.1175/JCLI-D-13-00454.1)